Inorganic Chemistry

pubs.acs.org/IC Article

Copper Bis(thiosemicarbazonato)-stilbenyl Complexes That Bind to Amyloid-β Plaques

Asif Noor, David J. Hayne, SinChun Lim, Jessica K. Van Zuylekom, Carleen Cullinane, Peter D. Roselt, Catriona A. McLean, Jonathan M. White, and Paul S. Donnelly*

Cite This: https://dx.doi.org/10.1021/acs.inorgchem.0c01520 Read Online

ACCESS | Metrics & More | Article Recommendations | Supporting Information

ABSTRACT: Alzheimer's disease is characterized by the presence of extracellular amyloid-β plaques. Positron emission tomography (PET) imaging with tracers radiolabeled with positron-emitting radionuclides that bind to amyloid-β plaques can assist in the diagnosis of Alzheimer's disease. With the goal of designing new imaging agents radiolabeled with positron-emitting copper-64 radionuclides that bind to amyloid-β plaques, a family of bis(thiosemicarbazone) ligands with appended substituted stilbenyl functional groups has been prepared. The ligands form charge-neutral and stable complexes with copper(II). The new ligands can be radiolabeled with copper-64 at room temperature. Two lead complexes were demonstrated to bind to amyloid-β plaques present in post-mortem brain tissue from subjects with clinically diagnosed Alzheimer's disease and crossed the blood-brain barrier in mice. The work presented here provides strategies to prepare compounds with radionuclides of copper that can be used for targeted brain PET imaging.

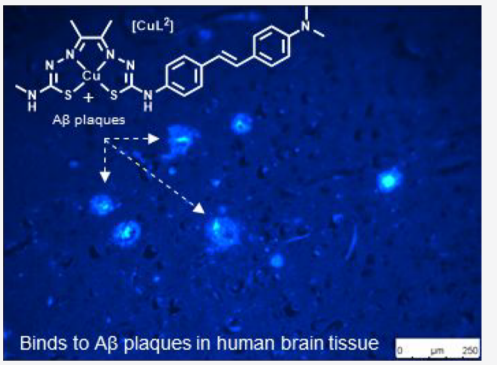

INTRODUCTION

Alzheimer's disease is characterized by the presence of extracellular amyloid plaques. The major constituent of these plaques are aggregated forms of the amyloid-β peptide (Aβ), a 39−43 amino acid peptide derived from the amyloid precursor protein.[1−5] The exact role amyloid plaques play in dementia remains controversial,[6] but noninvasive imaging of plaque burden using positron emission tomography (PET) is a useful tool to complement clinical and cognitive evaluation of patients.[7−10]

Appropriately substituted stilbene derivatives are conjugated, relatively planar, molecules that bind selectively to hydrophobic binding sites on amyloid-β aggregates through a combination of noncovalent interactions.[11,12] A stilbene derivative radiolabeled with fluorine-18, [^{18}F]florbetaben (Figure 1), has received clinical approval to detect the presence of amyloid and assist in diagnosis of Alzheimer's disease.[13] In this work we append a stilbene functional group to a copper chelator with the goal of developing amyloid imaging agents that can take advantage of positron-emitting copper radionuclides. Positron-emitting copper-64 has a radioactive half-life of 12.7 h, potentially facilitating delivery of tracers to facilities remote from the production site. Three other positron-emitting radionuclides of copper are also available. The relatively short-lived copper-62 radionuclide ($t_{1/2}$ = 9.7 min) can be provided by a ^{62}Zn/^{62}Cu generator system and has been used in brain imaging studies in humans.[14−17] Copper-60 ($t_{1/2}$ = 20 min) and copper-61 ($t_{1/2}$ = 3.4 h) can both be produced on biomedical cyclotrons in high purity.[18] A potential advantage of radiolabeling

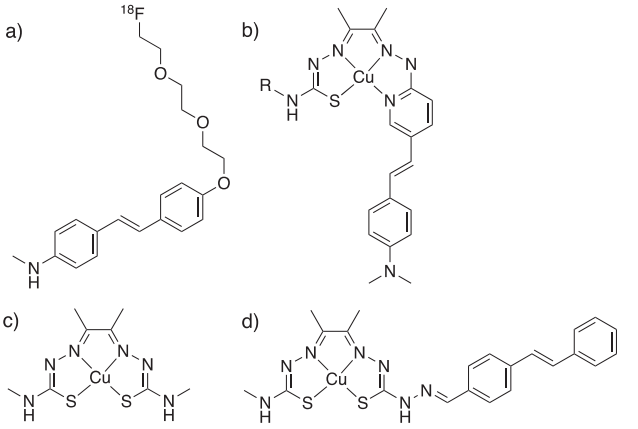

Figure 1. (a) [^{18}F]Florbetaben; (b) thiosemicarbazone-styrylpyridylhydrazone copper(II) complexes (R = CH_3 or $-(CH_2)_2N(CH_3)_2$);[19] (c) [Cu(atsm)]; and (d) [Cu(atsm/a-stilbene).[23]

Received: May 24, 2020

Scheme 1. Synthesis of [CuL$^{1\text{-}6}$]

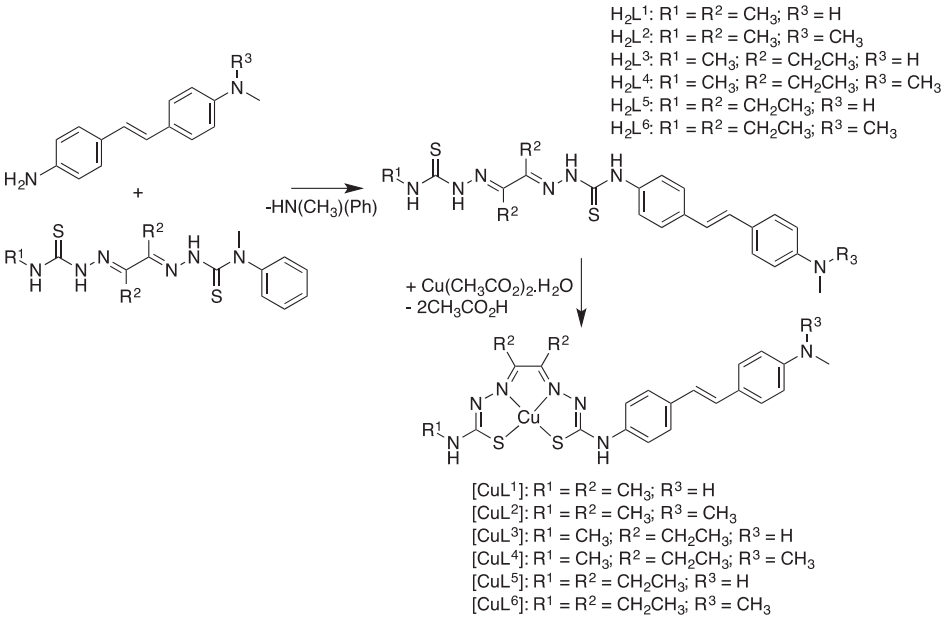

specifically designed ligands with copper radionuclides is the potential for the method to be a relatively simple alternative to the conventional organic synthesis required to incorporate fluorine-18 into tracers.

A challenge in developing copper-based brain amyloid imaging agents is designing copper complexes that are sufficiently stable and capable of crossing the blood−brain barrier. In an earlier work we developed hybrid thiosemicarbazone-pyridylhydrazone copper(II) complexes that incorporate a styrylpyridyl (Figure 1b) or pyridyl-benzofuran functional group and bind to amyloid-β plaques.[19,20] The thiosemicarbazone-styrylpyridylhydrazone copper complexes with a methyl functional group (Figure 1b; R = CH_3) bound to amyloid-β plaques in human brain tissue but did not cross the blood−brain barrier in mice. Modification of the terminal functional group to a $-CH_2CH_2N(CH_3)_2$ group (Figure 1b; R = $-CH_2CH_2N(CH_3)_2$) resulted in improved, but still modest, brain uptake in mice of 1.1 ± 0.2% injected activity/gram tissue (% IA/g).

In this manuscript, we extend our work on bis(thiosemicarbazone) ligands that are conjugated to stilbene functional groups with a goal of producing complexes which bind to amyloid-β plaques but have superior brain uptake. Tetradentate bis(thiosemicarbazone) ligands form charge-neutral and lipophilic complexes with copper radionuclides. One example, [Cu(atsm)] (Figure 1c), has been investigated as a hypoxia imaging agent and crosses the blood−brain barrier in humans.[14−17,21,22] In an earlier Communication, we reported a complex where a stilbene functional group was appended to a bis(thiosemicarbazone) ligand using a thiocarbohydrazone linkage, [Cu(atsm/a-stilbene)] (Figure 1d). The stilbene functional group in [Cu(atsm/a-stilbene)] is attached to the bis(thiosemicarbazone) ligand through a hydrazone linkage that was susceptible to hydrolysis, and this ligand proved relatively difficult to radiolabel with copper-64 with effective labeling, requiring transmetalation of the zinc(II) complex.[23]

In this work, we prepare a range of bis(thiosemicarbazone) ligands where a different synthetic methodology is used to append stilbene functional groups to bis(thiosemicarbazone) ligands. The complexes described in this work involve ligands where the stilbene functional group is directly attached to one thiosemicarbazone limb of the ligand through a stable N^4-substituted thiosemicarbazone functional group. The ability of the copper complexes to interact with synthetic amyloid-β_{1-40} and to bind to amyloid-β plaques in human brain tissue was investigated. Methods to make the radioactive copper-64 complexes were developed, and two candidates were selected for evaluation of their ability to cross the blood−brain barrier in mice.

RESULTS AND DISCUSSION

Small modifications to the ligand framework of bis(thiosemicarbazone) ligands affect the biological activity of their copper complexes.[21,24,25] For example, copper(II) complexes with electron-donating alkyl groups on the "diimine-like" backbone of the ligand have lower $Cu^{II/I}$ reduction potential and are therefore less susceptible to reduction when compared to complexes with hydrogen groups on the backbone.[26−30] The nature of the substituents on the backbone of bis(thiosemicarbazonato) copper(II) complexes can also alter lipophilicity, membrane permeability, and retention as well as altering noncovalent interactions with serum proteins.[31−35]

A family of bis(thiosemicarbazone) ligands with appended substituted stilbene functional groups were prepared with the goal of providing stable, charge-neutral copper complexes that could selectively bind to amyloid-β plaques. The binding of stilbene derivatives to amyloid-β plaques is favored by the addition of electron-donating substituents such as $-NHCH_3$ or $-N(CH_3)_2$. Complexes with modifications to the bis(thiosemicarbazones) ligand framework were prepared to investigate if these subtle changes can affect the ability of the complexes to cross the blood−brain barrier. For each ligand, alkyl (methyl or ethyl) functional groups remained on the diimine-like backbone of the ligand to retain the relative redox stability of [Cu(atsm)].

https://dx.doi.org/10.1021/acs.inorgchem.0c01520
Inorg. Chem. XXXX, XXX, XXX−XXX

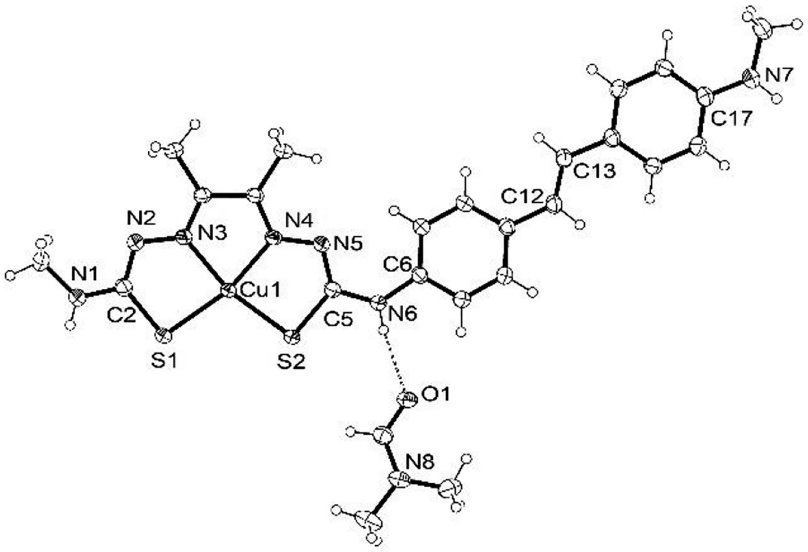

Figure 2. An ORTEP-3 representation of the crystal structure of [Cu**L**^{1}]. DMF (ellipsoids are shown at 40% probability). Bond lengths (Å), Cu1−S1 2.2473(6), Cu1−N3 1.961(2), C2−N1 1.337(3), C2−N2 1.318(3), C5−N5 1.321(3), C5−N6 1.354(3), C6−N6 1.409(2), C17−N7 1.383(3), C12−C13 1.335(3).

A family of six ligands, H_2L^{1-6}, were prepared by selective transamination reactions of substituted dissymmetric bis(thiosemicarbazone) precursors where one limb of the precursor bears one -*N4*-methyl-*N4*-phenyl-3-thiosemicarbazone functional group (Scheme 1).[36−39] Reaction of these precursors with primary amines, such as amino-stilbenes, involves nucleophilic attack of the primary amine on the thiocarbonyl carbon atom with the elimination of *N*-methylaniline to give the new ligands in excellent yields. In each case, the *E*-conformation of the double bond in the stilbene functional group was confirmed by ^{1}H NMR spectroscopy and a characteristic doublet ($^{3}J_{HH}$ = 17 Hz). The reaction of the ligands with copper(II) acetate monohydrate at room temperature allows isolation of red-brown charge-neutral copper(II) complexes. The electrospray ionization mass spectra all reveal signals that can be attributed to the protonated mono cations with the expected isotope patterns.

Absorption spectra of H_2L^{1-6} and [Cu**L**$^{1-6}$] (10 μM) were measured in phosphate buffered saline (pH 7.4) with 20% DMSO to assist in solubility. Each ligand and copper(II) complex has an absorbance at λ = 360 nm due to the functionalized stilbene. Complexation with copper(II) leads to an absorption at λ = 495 nm due to the characteristic metal−ligand-charge transfer transitions of bis(thiosemicarbazonato)-copper(II) complexes (Figure S21). The absorption spectra for Cu**L**$^{1-6}$ remain unchanged in the presence of a large excess of glutathione (1 mM, Figure S21) showing that the complexes are resistant to reduction and decomplexation in the presence of this abundant biological reductant and copper binding ligand.

It was possible to grow crystals of [Cu**L**^{1}] of suitable quality for analysis by X-ray crystallography. The X-ray crystal structure of [Cu**L**^{1}] (Figure 2) reveals that the copper(II) ion is in the expected distorted square planar environment with a dianionic tetradentate N_2S_2 ligand with three 5-membered chelate rings. The Cu−N bond lengths (Cu−N3 1.961(2) Å) and Cu−S (Cu1−S1 2.2473(6) Å) are similar to those found in [Cu(atsm)].[28,39,40] The double deprotonation of the ligand is evident with relatively short C2−N2 distance (1.318(3) Å), indicative of double bond character, and the C2−S1 distance (1.766(3) Å), indicative of more thiol-like rather than thione-like character.

Copper(II) bis(thiosemicarbazonato) complexes are stable (K_a = 10^{18}), but reduction to a copper(I) complex results in less stable complexes where copper(I) can dissociate from the ligand. The electrochemical properties of each of the complexes were investigated by cyclic voltammetry in anhydrous dimethylformamide. Each complex exhibited a quasi-reversible redox process at a glassy carbon electrode that could be attributed to a $Cu^{II/I}$ process ranging from E^m = −1.09 to E^m = −1.16 V vs ferricinium/ferrocene (Fc^+/Fc) (Figure 3, Table 1), similar to what is found in [Cu(atsm)] ($E^m \approx -1.16$ V). The similar reduction potentials of [Cu**L**$^{1-6}$] to [Cu(atsm)] suggest they should display a similar resistance to reduction *in vivo* as [Cu(atsm)].[26,29] Each complex also displayed two essentially irreversible and partially overlapping processes at more positive potentials, i.e., $E \sim 0-0.2$ V vs Fc^+/Fc. One of these processes may involve oxidation of the stilbene functional group as the free ligands show a similar oxidation (Figure S22). The second overlapping process could be due to either a $Cu^{III/II}$ process or oxidation of a ligand-based orbital with π-character on bis(thiosemicarbazonato) ligand (Figure 3). There is an oxidative process in [Cu(atsm)] at E^m = 0.15 V.[39,41,42]

The ligands H_2L^{1-6} could be radiolabeled with copper-64 at room temperature in 30 min to give [^{64}Cu][Cu**L**$^{1-6}$] in high radiochemical yields (>95%) without the need for further purification. The radiolabeled complexes were characterized by comparing their HPLC traces with their nonradioactive [$^{63/65}$Cu] analogues (Figure 4). The HPLC traces (C18 reversed phase column) of the compounds show a general trend of increased retention time with increasing molecular weight and expected lipophilicity, for example, [Cu**L**^{2}] (R^1 = R^2 = CH_3) has a shorter retention time than [Cu**L**^{6}] (R^1 = R^2 = CH_2CH_3) (Figure 4).

Estimations of lipophilicity made by measuring octanol−water partition coefficients (log *P*) or octanol-buffer distribution coefficients (log $D_{7.4}$) are often useful in identifying compounds that are likely to cross the blood−

https://dx.doi.org/10.1021/acs.inorgchem.0c01520
Inorg. Chem. XXXX, XXX, XXX−XXX

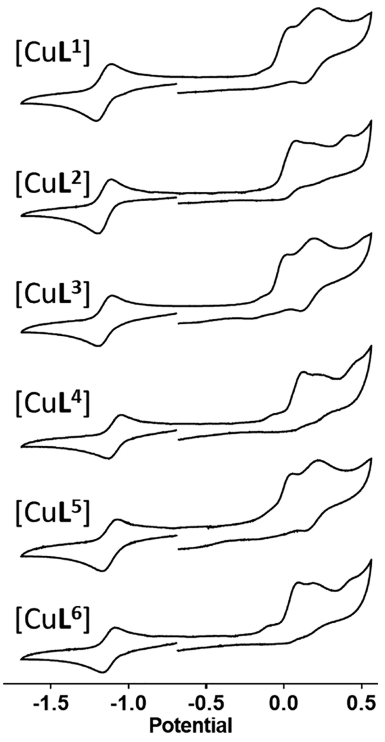

Figure 3. Cyclic voltammograms of $[CuL^{1-6}]$ in DMF at a glassy carbon working electrode, with a scan rate of 100 mV/s, 1 mM analyte, and electrolyte = 0.1 M $NBu_4^+PF_6^-$. Potentials quoted versus Fc^+/Fc.

Table 1. Summary of the $Cu^{II/I}$ Reduction Potentials of Complexes $[CuL^{1-6}]$

complex	E^m ($Cu^{II/I}$) vs (Fc^+/Fc)	I_c/I_a	peak separation (mV)
$[CuL^1]$	−1.16	1.14	95
$[CuL^2]$	−1.16	1.20	72
$[CuL^3]$	−1.15	1.15	76
$[CuL^4]$	−1.09	1.04	65
$[CuL^5]$	−1.14	1.41	81
$[CuL^6]$	−1.15	1.13	73

brain barrier through passive diffusion. Most compounds that cross the blood-brain barrier have a log(D) in the range of 1−3.[43−45] The log $D_{7.4}$ values for $[^{64}Cu][CuL^{1-6}]$ (Table 2) are all similar, ranging from 1.4−1.6. In this instance, this method is less able to discriminate complexes of similar lipophilicities than analysis by HPLC (Figure 4). The lipophilicity of each complex is within the range required for penetration of the blood−brain barrier and similar to that of [Cu(atsm)] (log $D_{7.4}$ = 1.49 ± 0.08)[46] which crosses the blood−brain barrier in humans,[14,15,47,48] although it is acknowledged that many other factors are also important such as efflux by P-glycoprotein.[49,50]

The dye Thioflavin-T (ThT, (2-[*p*-(dimethylamino)-phenyl]-3,6-dimethyl-benzothiaolium chloride) can be used to indicate the formation of $A\beta_{1-40}$ fibrils. The emission from ThT undergoes a λ = 115 nm red shift to λ_{em} = 485 nm upon interaction with amyloid fibrils. The incubation of a mixture of $A\beta_{1-40}$ (4 μM) and ThT (2 μM) in PBS at 37 °C leads to the formation of Aβ fibrils that can be monitored by measuring the increase in fluorescence from ThT (Figure 5a). Addition of $[CuL^{1-6}]$ (1 μM) results in a significant reduction in ThT fluorescence (Figure 5a). The reduced ThT fluorescence suggests that each of the complexes interact by $A\beta_{1-40}$ fibrils

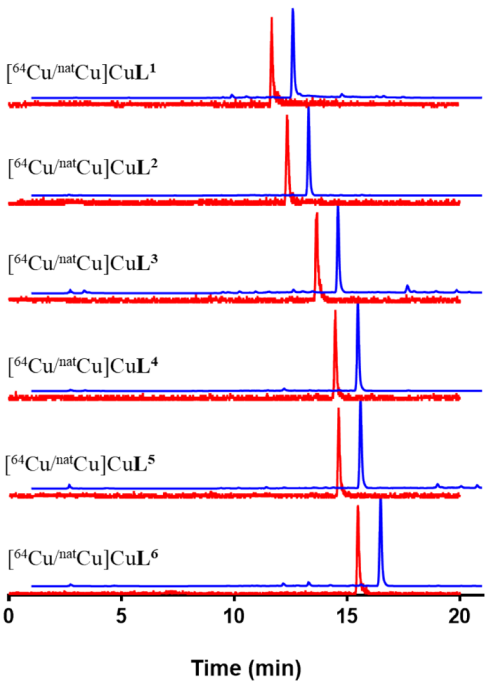

Figure 4. RP-HPLC chromatograms of $[^{64}Cu][CuL^{1-6}]$ (red) (radiation detection) and $[^{nat}Cu][CuL^{1-6}]$ (blue, λ_{abs} = 280 nm, offset for clarity).

Table 2. Log $D_{7.4}$ for $[^{64}Cu][CuL^{1-6}]$

complex	log $D_{7.4}$
$[^{64}Cu][CuL^1]$	1.6 ± 0.2
$[^{64}Cu][CuL^2]$	1.61 ± 0.01
$[^{64}Cu][CuL^3]$	1.5 ± 0.1
$[^{64}Cu][CuL^4]$	1.59 ± 0.05
$[^{64}Cu][CuL^5]$	1.44 ± 0.04
$[^{64}Cu][CuL^6]$	1.56 ± 0.03

either by binding directly to the fibrils in competition with ThT or by inhibiting fibril formation.

All six complexes displayed similar stability, $Cu^{II/I}$ reduction potentials, radiolabeling efficiency with copper-64, and log $D_{7.4}$ values, and all were shown to interact with $A\beta_{1-40}$, making the selection of two lead candidates for more detailed investigations somewhat arbitrary. A low molecular weight (<500 Da) is an important consideration for penetration of the blood−brain barrier,[45] which suggests that the complexes featuring the bis(thiosemicarbazone) framework with the lowest molecular weight, either CuL^1 or CuL^2 (Figure 2), would be worth further investigation. The complex where all the functional groups were methyl, $[CuL^2]$ (MW = 529 Da), was selected over $[CuL^1]$ based on the relative ease of synthesis of the dimethylamine-substituted stilbene precursor. The largest bis(thiosemicarbazone) framework, with all ethyl substituents on the bis(thiosemicarbazone) fragment, CuL^6 (MW = 571 Da), was also selected for further evaluation. The relatively simple switch of methyl to ethyl substituents on bis(thiosemicarbazone) copper(II) complexes can alter the extent to which the complexes bind to serum proteins which can also affect biodistribution, but this was not investigated in this work.[34,35,51]

The interactions of $[CuL^2]$ and $[CuL^6]$ with preformed mature Aβ fibrils were also investigated. A mixture of $A\beta_{1-40}$ (100 μM) was gently agitated in phosphate buffered saline

https://dx.doi.org/10.1021/acs.inorgchem.0c01520
Inorg. Chem. XXXX, XXX, XXX−XXX

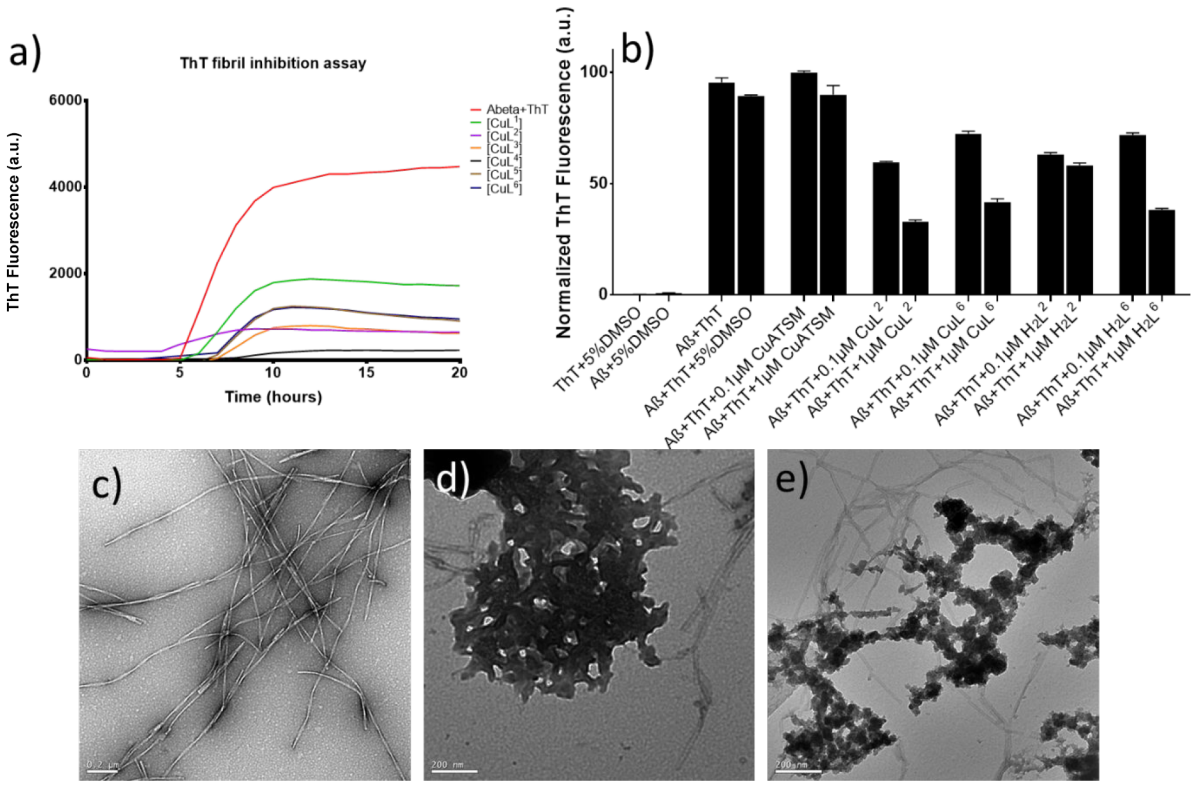

Figure 5. (a) Time-dependent changes in ThT fluorescence (λ_{ex} = 440 nm, λ_{em} = 480 nm) for solutions of Aβ_{1-40} (4 μM) and ThT (2 μM) incubated with and without Cu(II) complexes [Cu$\mathbf{L}^{1-6}$] (1 μM) over 20 h at 37 °C. (b) Aβ_{1-40} aggregation assay using mature fibrils (5 μM), where the data indicate the change in ThT fluorescence (5 μM) incubated for 1 h in the presence and absence of compounds. TEM micrographs of Aβ_{1-40} fibrils (10 μM) (c), Aβ_{1-40} fibrils (10 μM) in the presence of [Cu$\mathbf{L}^{2}$] (10 nM) (d), and Aβ_{1-40} fibrils (10 μM) in the presence of [Cu$\mathbf{L}^{6}$] (10 nM) (e).

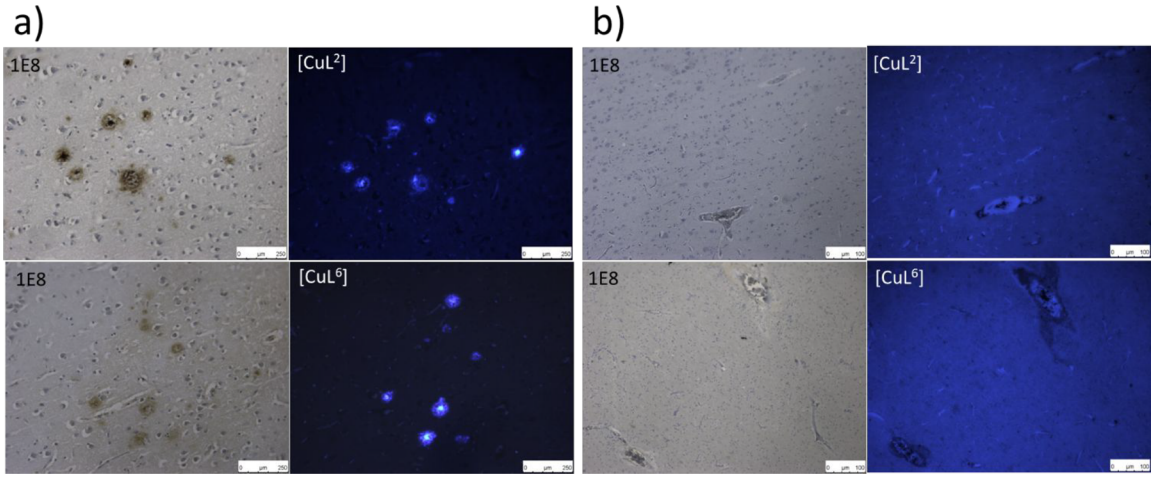

Figure 6. (a) Images of human brain tissue from an AD subject and (b) images of human brain tissue from aged-matched non-AD control. Images stained with 1E8 antibody were visualized with bright-field microscopy, and those of the contiguous section were stained with [Cu$\mathbf{L}^{2}$] or [Cu$\mathbf{L}^{6}$] and visualized using epi-fluorescence microscopy (λ_{ex} = 405 nm, λ_{em} = 461 nm).

(pH 7.4) at 37 °C for 48 h to promote the formation of Aβ_{1-40} fibrils and then ThT (100 μM) was added, and the mixture was incubated at 37 °C for a further 60 min. Aliquots of this mixture (5 μM fibrils) were then used for the following assays. An increase fluorescence (λ_{em} = 480 nm) from ThT confirmed the presence of Aβ_{1-40} fibrils, and the fluorescence intensity was similar to that in the presence of DMSO (5%) that is required to assist in the solubility of [Cu$\mathbf{L}^{1-6}$] (Figure 5 b). Addition of [Cu(atsm)] at either 0.1 μM or 1 μM did not significantly alter the emission intensity of ThT, suggesting no interaction with Aβ_{1-40} fibrils and that the presence of paramagnetic Cu^{II} (d^9) did not interfere with the assay. In contrast, addition of either [Cu$\mathbf{L}^{2}$] or [Cu$\mathbf{L}^{6}$] (0.1 μM) to Aβ_{1-40} fibrils (20 μM of fibrils, 20 μM ThT) resulted in a reduction in ThT fluorescence by 40% and 27%, respectively (Figure 5b), suggesting that the complexes are capable of binding to Aβ_{1-40} fibrils and displacing ThT. Addition of [Cu$\mathbf{L}^{2}$] and [Cu$\mathbf{L}^{6}$] at 1 μM of [Cu$\mathbf{L}^{2}$] and [Cu$\mathbf{L}^{6}$] resulted in

https://dx.doi.org/10.1021/acs.inorgchem.0c01520
Inorg. Chem. XXXX, XXX, XXX−XXX

a further reduction in fluorescent intensity from ThT by 67% and 58%, respectively (Figure 5b). The free ligands H_2L^2 and H_2L^6 were also capable of displacing ThT from Aβ_{1-40} fibrils, leading to similar reductions in fluorescence intensity as their respective metal complexes which provided further reassurance that the presence of paramagnetic copper(II) in the complexes does not interfere with the assay (Figure 5b).

The interaction of [Cu**L**^{2}] and [Cu**L**^{6}] with Aβ_{1-40} fibrils was also investigated using transmission electron microscopy (TEM). A mixture of Aβ_{1-40} (100 μM) was gently agitated for 48 h in phosphate buffered saline (pH 7.4) at 37 °C to promote the formation of Aβ fibrils, and then aliquots (10 μM) of fibrils were treated with either [Cu**L**^{2}] or [Cu**L**^{6}] for 2 h at 37 °C. The TEM images show the expected morphology of the fibrils (10 μM of fibrils) formed for the untreated sample (Figure 5c), while the images for the solutions treated with either [Cu**L**^{2}] or [Cu**L**^{6}] (10 μM of fibrils, 10 nM of complex) reveal a dramatic change in morphology to what appears to be amorphous irregular aggregates (Figure 5d, e).

The ligands H_2L^2 and H_2L^6 are fluorescent due to the presence of the stilbene functional group. Coordination of copper(II) to the ligands significantly reduces this fluorescence, but the copper(II) complexes remain sufficiently fluorescent (λ_{em} = 440 nm, λ_{ex} = 365 nm, Figure S20) to detect their binding to amyloid-β plaques in brain tissue using epi-fluorescence microscopy. Post-mortem samples of frontal cortex of human brain tissue (7 μm serial sections) from clinically diagnosed Alzheimer's disease subjects were pretreated with 2% bovine serum albumin to reduce nonspecific binding and then treated with either [Cu**L**^{2}] or [Cu**L**^{6}] (10 μM). The selective retention of the complexes on the treated brain tissue was assessed using epi-fluorescence microscopy (λ_{ex} = 405 nm, λ_{em} = 461 nm, Figure 6). Amyloid-β plaques are typically 40−60 μm in diameter, so contiguous serial sections of tissue (7 μm) often contain portions of the same plaque. The complexes bound selectively to amyloid-β plaques that could be identified by comparison with the contiguous section of tissue where the amyloid-β plaques had been stained with an amyloid-β specific antibody (1E8). Importantly, neither [Cu**L**^{2}] or [Cu**L**^{6}] showed any evidence of significant retention on brain tissue from age-matched control subjects (non-AD post-mortem tissue, Figure 6).

The potential of [^{64}Cu][Cu**L**^{2}] and [^{64}Cu][Cu**L**^{6}] to cross the blood−brain barrier was evaluated in wild-type mice (Balb/c). The radiolabeled tracers were administered via tail vein injection, and then the mice were euthanized at either 2 or 60 min postinjection. The activity accumulated in each organ was counted and expressed as a percentage of the injected activity normalized to the mass of the organ (% IA/g). Both the tracers show good brain uptake after 2 min postinjection, [^{64}Cu**L**^{2}] = 2.2 ± 0.6% IA/g; [^{64}Cu**L**^{6}] = 1.1 ± 0.2% IA/g (Figure 7 and Table 3). For both compounds the degree of brain uptake is similar to that of [^{64}Cu]Cu(atsm) in wild-type mice (~0.9 ± 0.4% ID/g)[52] which correlates to sufficient uptake for imaging the brain in humans. Wild-type mice do not possess Aβ plaques, so an ideal tracer should clear from their brains rather than be retained.[12] Following the initial uptake in the brain, both tracers display good clearance at 60 min postinjection ([^{64}Cu**L**^{2}] = 0.34 ± 0.04% IA/g; [^{64}Cu**L**^{6}] = 0.22 ± 0.02% IA/g). The high level of uptake in the liver for both compounds is expected for lipophilic compounds that clear primarily through hepatobiliary metabolism.[53,54] The high degree of uptake in the lungs at 2 min postinjection for both compounds could be related to the large blood volume in the lungs and could relate to the activity present in blood.[55]

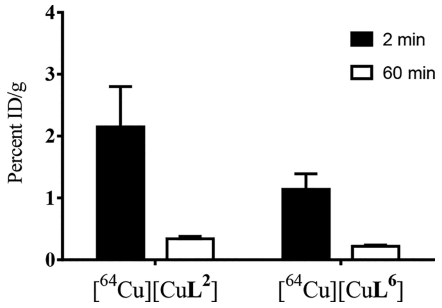

Figure 7. Brain uptake measured by an ex-vivo biodistribution analysis. Mice were euthanized at 2 and 60 min after injection. Tissues were harvested, weighed, and radioactivity quantified on a gamma counter. Brain uptake expressed as % injected dose/gram tissue. Data represents mean ± SEM of n = 3 mice/group.

Table 3. Biodistribution Data Expressed as Injected Activity Normalized to the Mass of the Organ (% IA/g)[a]

	[^{64}Cu][Cu**L**^{2}]		[^{64}Cu][Cu**L**^{6}]	
	2 min	60 min	2 min	60 min
blood	22.0(2.4)	1.8(0.1)	16.8(2.7)	1.5(0.1)
lungs	95.5(20.4)	14.3(3.5)	67.4(7.7)	29.7(5.1)
heart	13.8(1.7)	3.8(0.3)	13.1(2.9)	2.3(0.1)
liver	35.5(2.3)	50.8(1.2)	50.3(4.2)	67.9(2.9)
kidneys	7.0(0.3)	8.2(0.5)	7.8(0.5)	4.3(0.2)
muscle	1.0(0.1)	1.2(0.1)	0.7(0.1)	0.49(0.01)
spleen	16.1(0.9)	33.0(2.0)	59.7(22.5)	125.9(12.8)
brain	2.2(0.6)	0.34(0.04)	1.1 (0.2)	0.22(0.02)

[a]Standard error given in brackets (n = 3).

CONCLUSION

Amyloid imaging agents that use the range of positron-emitting radionuclides of copper that are available could increase the number of facilities that could perform diagnostic PET scans.[19,20,23,56−62] Incorporating positron-emitting radionuclides of copper(II) into specifically designed ligands can be relatively simple, fast, and efficient when compared to the incorporation of fluorine-18 into organic molecules through the formation of covalent C−F bonds. However, a major challenge in using metal complexes for brain imaging applications is the difficulty in preparing metal complexes that cross the blood−brain barrier yet retain selectivity for particular targets. In this work a family of bis(thiosemicarbazone) ligands with appended substituted stilbene ligands have been prepared that form charge-neutral and stable complexes with copper(II). The new ligands could be radiolabeled with [^{64}Cu]Cu^{II} at room temperature, and the complexes have a lipophilicity, as estimated by measurements of log $D_{7.4}$, within a range that is consistent with compounds that cross the blood−brain barrier. Two leads complexes, that were selected for further evaluation, bound to amyloid plaques present in post-mortem brain tissue for AD subjects. These two compounds cross the blood−brain barrier in mice to a similar degree to [^{64}Cu][Cu(atsm)],[52] a complex that has been used for brain imaging in humans.[14−17,48]

The brain uptake of [^{64}Cu][Cu**L**^{2}] is better than the copper(II) hybrid thiosemicarbazone-styrylpyridylhydrazone copper complexes with a $-CH_2CH_2N(CH_3)_2$ functional

https://dx.doi.org/10.1021/acs.inorgchem.0c01520
Inorg. Chem. XXXX, XXX, XXX−XXX

group (Figure 1b; R = $-CH_2CH_2N(CH_3)_2$) that we reported previously.[19] The ligands presented in this work are easier to radiolabel than the H_2atsm/a-stilbene derivative (Figure 1d) we reported in a preliminary Communication.[23] A direct comparison of the brain uptake for [^{64}Cu][Cu**L**^{2}] and [^{64}Cu]Cuatsm/a-stilbene (Figure 1d) is not possible because a different method of quantification (PET imaging) was used in the earlier work.[23]

Future work on the complexes described here could include investigating their uptake and retention in murine models of amyloid pathology and quantifying their affinity for amyloid-β_{1-40}. An advantage of ligands designed to bind copper(II) is that it is possible to use them for any of the four positron-emitting radionuclides of copper that are available. This work focused on copper-64, but extrapolation of this chemistry to copper-60, copper-61, or copper-62 should be relatively straightforward. The ligands described here could be readily adapted to kit-based formulations, similar to those for diagnostic agents based on technetium-99.

EXPERIMENTAL SECTION

General Procedures. Unless otherwise stated, all reagents were purchased from commercial sources and used without further purification. Flash column chromatography was carried out using silica gel (40−63 μm) as the stationary phase. Analytical TLC was performed on precoated silica gel plates (0.25 mm thick, 60F254, Merck, Germany) and visualized under UV light. ^{1}H and ^{13}C NMR spectra were recorded either on a 400 MHz Varian/Agilent 400-MR or 500 MHz AR spectrometer at 298 K. Chemical shifts are reported in parts per million (ppm) and referenced to the residual solvent peak. Coupling constants (J) are reported in Hertz (Hz). Standard abbreviations indicating multiplicity were used as follows: m = multiplet, quint. = quintet, q = quartet, t = triplet, d = doublet, s = singlet, br = broad. ESI-MS spectra were recorded on an Agilent 6510 ESI-TOF LC/MS mass spectrometer or a Thermo Fisher OrbiTRAP infusion mass spectrometer. 4-Methyl-4-phenyl-3-thiosemicarbazide,[63] 4-methylaminobenzaldehyde,[64] and H_2-ATSM/M_2[36] were prepared according to reported procedures. UV−vis spectroscopy was performed on a Shimadzu UV1650-PC spectrometer (Shimadzu, Kyoto, Japan), and a Varian Cary Eclipse fluorescence spectrometer was used for fluorescence spectroscopy. Cyclic voltammograms were recorded using a Metrohm (Switzerland) AUTOLAB PGSTAT100 instrument and analyzed using Autolab GPES V4.9 software. Measurements were carried out using 1 mM analyte in anhydrous DMF with tetrabutylammonium hexafluorophosphate (0.1 M) as a supporting electrolyte. A glassy carbon working electrode was used along with a Pt wire counter electrode and a pseudo-leakless Ag/Ag$^+$ working electrode (EDAQ, New South Wales, Australia). Measurements were referenced to internal ferrocene (Fc/Fc$^+$, E^m = 0.00 V where E^m = (Epc + Epa)/2.

Synthesis of (*E*)-4-Nitro-4′-methylaminostilbene. 4-Nitrobenzyl phosphanate (2.1 g, 7.7 mmol) was dossolved in dimethylformamide (dry, 10 mL), and then sodium hydride (60% w/w in mineral oil, 0.39 g, 9.8 mmol) was added. The suspension was stirred for 15 min followed by the addition of 4-methylaminobenzaldehyde (0.94 g, 7.0 mmol). The mixture was stirred for 2 h, and then ethanol (2 mL) was added, followed by dH_2O (50 mL), to afford a red precipitate. The precipitate was isolated by filtration and washed with dH_2O. The red solid was dissolved in dichloromethane and washed with dH_2O (3 × 200 mL) and then brine (1 × 100 mL). The organic phase was dried ($MgSO_4$) and filtered, and the solvent was removed under reduced pressure to afford a red solid (1.4 g, 5.5 mmol, 79%). ^{1}H NMR (400 MHz; $CDCl_3$): δ 8.18 (m, 2H, Ar*H*), 7.56 (m, 2H, Ar*H*), 7.41 (m, 2H, Ar*H*), 7.19 (d, $^3J_{HH}$ = 16.2 Hz, 1H, CH═C*H*), 6.92 (d, $^3J_{HH}$ = 16.2 Hz, 1H, C*H*═CH), 6.60 (m, 2H, Ar*H*), 3.98 (br, J = 0.5 Hz, 1H, N*H*), 2.89 (s, 3H, CH_3). ^{13}C NMR (101 MHz; $CDCl_3$): δ 150.1, 133.9, 128.7, 126.2, 125.5, 124.3, 121.8, 112.5, 30.6. HRMS (ESI) (+ve ion) m/z calcd for $[C_{15}H_{17}N_2O_2]^+$: 255.11 [M + H]$^+$; found, 255.113.

Synthesis of (*E*)-4-Amino-4′-methylaminostilbene. To (*E*)-4-nitro-4′-methylaminostilbene (0.99 g, 3.9 mmol) was added ethanol (20 mL), and the mixture was sparged with N_2 (1 h). Stannous chloride was then added (4.40 g, 23 mmol) to the mixture, and the mixture was heated at reflux. After 1.5 h, the reaction was cooled to ambient temperature and adjusted to pH 9 (1 M NaOH). The mixture was extracted into ethyl acetate (3 × 80 mL), and the combined organic phase was washed with brine (3× 100 mL), dried ($MgSO_4$), and filtered; the solvent was then removed under reduced pressure to afford a yellow solid (0.75 g, 3.3 mmol, 87%). ^{1}HNMR (400 MHz; CDCl3): δ 7.32 (m, 4H, Ar*H*), 6.86 (m, 2H, CH_2═CH_2), 6.67 (m, 2H, Ar*H*), 6.60 (m, 2H, Ar*H*), 3.68 (s, 3H, NH_2, N*H*Me), 2.86 (s, 3H). ^{13}C NMR (101 MHz; $CDCl_3$): δ 148.6, 145.5, 129.0, 127.48, 127.36, 127.28, 125.6, 124.7, 115.4, 112.6, 30.9. HRMS (ESI) (+ve ion) m/z calcd for $[C_{15}H_{17}N_2O_2]^+$: 225.14 [M + H]$^+$; found, 225.137.

Synthesis of (*E*)-4-Nitro-4′-dimethylaminostilbene. To 4-nitrobenzyl phosphanate was added dimethylformamide (dry, 10 mL), and the mixture was stirred under an atmosphere of N_2. To the dark yellow solution was added sodium hydride (60% w/w in mineral oil, 0.41 g, 10 mmol), and the mixture became dark red in color. After 15 min, 4-dimethylbenzaldehyde was added to the reaction mixture and the mixture was stirred for 1 h. Ethanol was added (2 mL) to this mixture and then dH_2O (50 mL) was added to afford a red precipitate.The precipitate was isolated by filtration and washed with dH_2O. The red solid was dissolved in dichloromethane and washed with dH_2O (3 × 200 mL) and then brine (1 × 100 mL). The organic phase was dried ($MgSO_4$) and filtered, and the solvent was removed under reduced pressure to afford a red solid (1.75 g, 6.5 mmol, 90%). ^{1}H NMR (400 MHz; $CDCl_3$): δ 8.18 (m, 2H, Ar*H*), 7.56 (m, 2H, Ar*H*), 7.45 (m, 2H, Ar*H*), 7.21 (d, $^3J_{HH}$ = 16.2, 1H, C*H*═CH), 6.93 (d, $^3J_{HH}$ = 16.2, 1H, CH═C*H*), 6.72 (m, 2H, Ar*H*), 3.02 (s, 6H, N(CH_3)$_2$). ^{13}C NMR (101 MHz; $CDCl_3$): δ 151.0, 145.2, 133.8, 128.5, 126.2, 124.43, 124.30, 121.7, 112.3, 40.4. HRMS (ESI) (+ve ion) m/z calcd for $[C_{16}H_{17}N_2O_2]^+$: 269.32 [M + H]$^+$; found, 269.129.

Synthesis of (*E*)-4-Amino-4′-dimethylaminostilbene. To (*E*)-4-nitro-4′-dimethylaminostilbene (1.7 g, 6.5 mmol) was added ethanol (40 mL), and the mixture was sparged with N_2 (1 h). Stannous chloride was added (7.6 g, 40 mmol) to this mixture, and the mixture was heated at reflux. After 1.5 h, the reaction was cooled to ambient temperature and adjusted to pH 9 (1 M NaOH). The mixture was extracted into dichloromethane (300 mL), and the organic phase was washed with brine (150 mL), dried ($MgSO_4$), and filtered; the solvent was then removed under reduced pressure to afford a yellow solid (1.1 g, 4.6 mmol, 71%). ^{1}H NMR (400 MHz; CDCl3): δ 7.38 (m, 2H, ArH), 7.30 (m, 2H, ArH), 6.86 (m, 2H, CH═CH), 6.72 (m, 2H, ArH), 6.67 (m, 2H, ArH), 3.67 (br, 2H, NH_2), 2.97 (s, 6H, N(CH_3)$_2$). ^{13}C NMR (101 MHz; $CDCl_3$): δ 149.9, 145.5, 129.1, 127.30, 127.22, 126.7, 125.5, 124.8, 115.4, 112.8, 40.7. HRMS (ESI) (+ve ion) m/z calcd for $[C_{16}H_{19}N_2]^+$: 239.15 [M + H]$^+$; found, 239.15.

Synthesis of (*E*)-*N*-Methyl-2-(4-oxohexan-3-ylidene)-hydrazine-1-carbothioamide. To a flask charged with 3,4-hexadione (7.827 g, 68.6 mmol) was added dH_2O (200 mL) and a catalytic amount of acetic acid (5 drops). The mixture was cooled to 5 °C and 4-methyl-3-thiosemicarbazide (6.086 g, 57.9 mmol) was added in portions over 2 h. A white precipitate was observed, and the mixture was stirred for 1 h further after the final addition. The white precipitate was isolated by filtration, washed with dH_2O and then pentane, and dried at the pump (quantitative yield). ^{1}H NMR (400 MHz; DMSO-d_6): δ 10.81 (s, 1H, N*H*), 8.56 (m, 1H, N*H*), 3.05 (d, $^3J_{HH}$ = 4.5 Hz, 3H, CH_3), 2.95 (q, $^3J_{HH}$ = 7.3 Hz, 2H, CH_2), 2.59 (q, $^3J_{HH}$ = 7.5 Hz, 2H, CH_2), 0.97 (t, $^3J_{HH}$ = 7.3 Hz, 3H, CH_3), 0.86 (t, $^3J_{HH}$ = 7.5 Hz, 3H, CH_3). ^{13}C NMR (101 MHz; DMSO-d_6): δ 200.0, 179.0, 149.0, 31.4, 29.3, 16.4, 10.2, 8.1; HRMS (ESI) (+ve ion) m/z calcd for $[C_8H_{16}N_3OS]^+$: 202.10 [M + H]$^+$; found, 202.101.

Synthesis of (*E*)-*N*-Ethyl-2-(4-oxohexan-3-ylidene)-hydrazine-1-carbothioamide. To a flask charged with 3,4-

https://dx.doi.org/10.1021/acs.inorgchem.0c01520
Inorg. Chem. XXXX, XXX, XXX−XXX

hexadione (7.107 g, 62.3 mmol) was added dH_2O (200 mL) and a catalytic amount of acetic acid (5 drops). The mixture was cooled to 5 °C and 4-ethyl-3-thiosemicarbazide (6.104 g, 51.2 mmol) was added in portions over 2 h. A white precipitate was observed, and the mixture was stirred for 1 h further after the final addition. The white precipitate was isolated by filtration, washed with dH_2O and then pentane, and dried at the pump (quantitative yield). ^{1}H NMR (400 MHz; DMSO-d_6): δ 10.74 (s, 1H, N*H*), 8.59 (m, 1H, N*H*), 3.62 (m, 3H, CH_2), 2.95 (q, $^3J_{HH}$ = 7.3 Hz, 2H, CH_2), 2.59 (q, $^3J_{HH}$ = 7.5 Hz, 2H, CH_2), 1.16 (t, $^3J_{HH}$ = 7.1 Hz, 3H, CH_3), 0.98 (t, $^3J_{HH}$ = 7.3 Hz, 3H, CH_3), 0.86 (t, $^3J_{HH}$ = 7.5 Hz, 3H, CH_3). ^{13}C NMR (101 MHz; DMSO-d_6): δ 8.08, 10.18, 14.11, 16.45, 29.32, 38.75, 148.99, 178.03, 199.90. HRMS (ESI) (+ve ion) m/z calcd for $[C_9H_{18}N_3OS]^+$: 216.12 $[M + H]^+$; found, 216.117.

Synthesis of DTSM-*N*-methyl-*N*-phenyl. To a flask charged with 4-methyl-4-phenyl-3-thiosemicarbazide (1.506 g, 8.3 mmol) and (*E*)-*N*-methyl-2-(4-oxohexan-3-ylidene)hydrazine-1-carbothioamide (1.664, 8.3 mmol) was added EtOH (50 mL) and a catalytic amount of acetic acid (8 drops). The mixture was heated at reflux for 1.5 h. A white precipitate was observed and was collected by filtration after the reaction cooled to ambient temperature. The precipitate was washed with a minimum of ethanol and then pentane and dried at the pump. Additional product was collected after the filtrate was stirred at ambient temperature over 48 h (1.211 g, 3.3 mmol, 40%). ^{1}H NMR (500 MHz, DMSO-d_6): δ 11.08 (s, 3H, N*H*), 10.40 (s, 1H), 9.35 (d, J = 5.1 Hz, 1H, N*H*), 8.30 (q, J = 4.3 Hz, 1H, N*H*), 7.60−7.48 (m, 2H, Ar*H*), 7.40 (dd, J = 12.4, 4.7 Hz, 3H, Ar*H*), 3.56 (s, 3H, CH_3), 3.03 (d, 3H, CH_3), 2.96−2.76 (m, 4H, CH_2CH$_3$), 1.00−0.79 (m, 6H, CH$_2$CH_3). ^{13}C NMR (126 MHz, DMSO-d_6): δ 178.99, 175.08, 169.15, 150.51, 143.37, 130.47, 128.44, 127.13, 43.28, 31.75, 17.67, 17.56, 11.55, 11.48. HRMS (ESI) (+ve ion) m/z calcd for $[C_{16}H_{25}N_6S_2]^+$: 356.1582 $[M + H]^+$; found, 365.1575

Synthesis of DTSE-*N*-methyl-*N*-phenyl. To a flask charged with 4-methyl-4-phenyl-3-thiosemicarbazide (1.521 g, 8.4 mmol) and (*E*)-*N*-ethyl-2-(4-oxohexan-3-ylidene)hydrazine-1-carbothioamide (1.807, 8.4 mmol) was added EtOH (50 mL) and a catalytic amount of acetic acid (6 drops). The mixture was heated until the reagents had dissolved and then was left to stir at ambient temperature for 72 h. A white precipitate was observed and was collected by filtration, washed with a minimum of ethanol and then pentane, and dried at the pump. Additional product was collected after the filtrate was stirred at ambient temperature over 48 h (1.370 g, 3.62 mmol, 43%). ^{1}H NMR (400 MHz; DMSO-d_6): δ 11.09 (s, 1H, N*H*), 10.40 (s, 1H), 9.34 (d, J = 4.3 Hz, 1H, N*H*), 8.29 (t, J = 5.8 Hz, 1H, N*H*), 7.51 (m, 2H, Ar*H*), 7.39 (m, 3H, Ar*H*), 3.58 (m, 5H, CH_3, CH_2CH$_3$), 2.84 (m, 4H, CH_2CH$_3$), 1.12 (t, $^3J_{HH}$= 7.1 Hz, 3H), 0.90 (m, 6H, CH$_2$CH_3). ^{13}C NMR (126 MHz; DMSO-d_6): δ 178.8, 177.5, 174.6, 152.5, 150.0, 142.8, 130.0, 128.0, 126.7, 42.8, 38.6, 17.2, 14.3, 11.07, 11.03. HRMS (ESI) (+ve ion) m/z calcd for $[C_{17}H_{27}N_6S_2]^+$: 379.1739 $[M + H]^+$; found, 379.1733

Synthesis of H_2L^1. To a flask charged with H_2ATSM-M_2 (0.24 g, 0.88 mmol) and (*E*)-4-amino-4′-methylaminostilbene (0.20 g, 0.88) was added acetonitrile (17 mL). The reaction was heated at reflux for 18 h, and an orange precipitate was observed. The precipitate was isolated from the hot reaction mixture by filtration, washed with acetonitrile and then diethyl ether, and dried *in vacuo* to afford an orange powder (0.28 g, 0.63 mmol, 72%). ^{1}H NMR (400 MHz; DMSO-d_6): δ 10.57 (s, 1H, N*H*), 10.30 (s, 1H, N*H*), 9.94 (s, 1H, N*H*), 8.41 (m, 1H, N*H*), 7.56 (m, 2H, Ar*H*), 7.50 (m, 2H, Ar*H*), 7.35 (m, 2H, Ar*H*), 7.07 (d, $^3J_{HH}$ = 16.3 Hz, 1H, C*H*═CH), 6.91 (d, $^3J_{HH}$ = 16.3 Hz, 1H, CH═C*H*), 6.54 (d, $^3J_{HH}$ = 8.6 Hz, 2H, Ar*H*), 5.88 (m, 1H, N*H*), 3.04 (d, $^3J_{HH}$ = 4.5 Hz, 3H, CH_3), 2.70 (d, $^3J_{HH}$ = 5.0 Hz, 3H, CH_3), 2.29 (s, 3H, CH_3), 2.25 (s, 3H, CH_3). ^{13}C NMR (101 MHz; DMSO): δ 11.78, 12.05, 29.60, 31.24, 111.65, 122.24, 124.57, 125.34, 125.39, 127.59, 128.77, 135.18, 137.25, 147.74, 149.24, 149.71, 176.42, 178.49. HRMS (ESI) (+ve ion) m/z calcd for $[C_{22}H_{28}N_7S_2]^+$: 454.1848 $[M + H]^+$; found, 454.1849. Elemental analysis calcd (%) for $C_{22}H_{27}N_7S_2.0.5H_2O$: C 57.12, H 6.10, N 21.19; found C 57.07, H 6.05, N 21.15.

Synthesis of H_2L^2. To a flask charged with H_2ATSM-M_2 (0.23, 0.82 mmol) and (*E*)-4-amino-4′-dimethylaminostilbene (0.20 g, 0.84) was added acetonitrile (17 mL). The reaction was heated at reflux for 18 h, and an orange precipitate was observed. The precipitate was isolated from the hot reaction mixture by filtration, washed with acetonitrile and then diethyl ether, and dried *in vacuo* (0.26 g, 0.56 mmol, 67%). ^{1}H NMR (400 MHz; DMSO-d_6): δ 10.58 (s, 1H, N*H*), 10.30 (s, 1H, N*H*), 9.94 (s, 1H, N*H*), 8.41 (d, J = 4.5 Hz, 1H), 7.54 (q, J = 11.7 Hz, 4H), 7.43 (d, J = 8.8 Hz, 2H), 7.11 (d, J = 16.3 Hz, 1H), 6.97 (d, J = 16.4 Hz, 1H), 6.73 (d, J = 8.9 Hz, 2H), 3.04 (d, J = 4.5 Hz, 3H), 2.93 (s, 6H), 2.29 (s, 3H), 2.25 (s, 3H). ^{13}C NMR (126 MHz, DMSO-d_6): δ 178.94, 176.86, 150.38, 149.71, 148.19, 137.84, 135.49, 128.85, 127.91, 125.91, 125.83, 125.44, 123.49, 112.70, 31.69, 12.50, 12.23. HRMS (ESI) (+ve ion) m/z calcd for $[C_{23}H_{30}N_7S_2]^+$: 468.2004 $[M + H]^+$; found, 468.1993.

Synthesis of H_2L^3. To a flask charged with DTSM-*N*-methyl-*N*-phenyl (334 mg, 0.92 mmol) and (*E*)-4-amino-4′-methylaminostilbene (206 mg, 0.92 mmol) was added acetonitrile (10 mL), and the mixture was heated at reflux for 6 h. A yellow precipitate was isolated by hot filtration, washed with acetonitrile and then pentane, and dried *in vacuo* (133 mg, 0.30 mmol, 33%). ^{1}H NMR (400 MHz; DMSO-d_6): δ 10.73 (s, 1H, N*H*), 10.44 (s, 1H, N*H*), 9.88 (s, 1H, N*H*), 8.33 (m, 1H, N*H*), 7.57 (m, 2H, Ar*H*), 7.50 (m, 2H, Ar*H*), 7.35 (m, 2H, Ar*H*), 7.07 (d, $^3J_{HH}$ = 16.4 Hz, 1H, C*H*═CH), 6.91 (d, $^3J_{HH}$ = 16.4 Hz, 1H, CH═C*H*), 6.54 (m, 2H, Ar*H*), 5.88 (m, 1H, N*H*), 3.03 (m, 3H, CH_3), 2.95 (m, 4H, 2CH_2), 2.70 (m, 3H, CH_3), 0.94 (m, 6H, 2CH_3). ^{13}C NMR (126 MHz; DMSO-d_6): δ 178.5, 176.3, 152.1, 150.6, 149.7, 137.2, 135.2, 128.8, 127.6, 125.4, 125.0, 124.6, 122.2, 111.7, 31.3, 29.6, 17.19, 17.14, 11.00, 10.82. HRMS (ESI) (+ve ion) m/z calcd for $[C_{24}H_{32}N_7S_2]^+$: 482.2161 $[M + H]^+$; found, 482.2153. Elemental analysis calcd (%) for $C_{24}H_{31}N_7S_2{\cdot}1.2H_2O{\cdot}$MeCN: C 57.37, H 6.74, N 20.58; found C 57.25, H 6.40, N 20.59.

Synthesis of H_2L^4. To a flask charged with DTSM-*N*-methyl-*N*-phenyl (94 mg, 0.26 mmol) and (*E*)-4-amino-4′-dimethylaminostilbene (62 mg, 0.26 mmol) was added acetonitrile (5 mL), and the mixture was heated at reflux for 6 h. A yellow precipitate was isolated by hot filtration, washed with acetonitrile and then pentane, and dried *in vacuo* (30 mg, 0.06 mmol, 24%). ^{1}H NMR (400 MHz; DMSO-d_6): δ 10.73 (s, 1H, N*H*), 10.44 (s, 1H, N*H*), 9.89 (s, 1H, N*H*), 8.32 (m, 1H, N*H*), 7.59 (m, 2H, Ar*H*), 7.52 (m, 2H, Ar*H*), 7.43 (m, 2H, Ar*H*), 7.11 (d, $^3J_{HH}$= 16.3 Hz, 1H, C*H*═CH), 6.97 (d, $^3J_{HH}$ = 16.3 Hz, 1H, CH═C*H*), 6.73 (m, 2H, Ar*H*), 3.04 (d, $^3J_{HH}$ = 4.4 Hz, 3H, CH_3), 2.98 (m, 10H, 2CH_2, N(CH_3)$_2$), 0.95 (m, 6H, 2CH_3). ^{13}C NMR (101 MHz; DMSO-d_6): δ 178.5, 176.3, 152.1, 150.7, 149.9, 137.3, 135.0, 128.4, 127.5, 125.5, 125.02, 124.99, 123.0, 112.2, 40.0, 31.3, 17.21, 17.15, 11.01, 10.83. HRMS (ESI) (+ve ion) m/z calcd for $[C_{25}H_{34}N_7S_2]^+$: 496.2317 $[M + H]^+$; found, 496.2311. Elemental analysis calcd (%) for $C_{25}H_{33}N_7S_2{\cdot}0.7H_2O$: C 59.07, H 6.82, N 19.29; found C 58.75, H 6.40, N, 19.48.

Synthesis of H_2L^5. To a flask charged with DTSE-*N*-methyl-*N*-phenyl (80 mg, 0.21 mmol) and (*E*)-4-amino-4′-methylaminostilbene (50 mg, 0.22 mmol) was added acetonitrile (5 mL), and the mixture was heated at reflux for 6 h. A yellow precipitate was isolated by hot filtration, washed with acetonitrile and then pentane, and dried *in vacuo* (33 mg, 0.07 mmol, 32%). ^{1}H NMR (400 MHz; DMSO-d_6): δ 10.75 (s, 1H, N*H*), 10.39 (s, 1H, N*H*), 9.88 (s, 1H, N*H*), 8.33 (m, 1H, N*Hz*), 7.57 (m, 2H, Ar*H*), 7.50 (m, 2H, Ar*H*), 7.35 (m, 2H, Ar*H*), 7.07 (d, $^3J_{HH}$ = 16.3 Hz, 1H, C*H*═CH), 6.91 (d, $^3J_{HH}$ = 16.3 Hz, 1H, CH═C*H*), 6.54 (m, 2H, Ar*H*), 5.88 (m, 1H, N*H*), 3.60 (m, 2H, CH_2), 2.97−2.87 (m, 4H, 2CH_2), 2.70 (m, 3H, CH_3), 1.15 (m, 3H, CH_3), 0.93 (m, 6H, 2CH_3). ^{13}C NMR (101 MHz; DMSO-d_6): δ 177.9, 176.7, 152.4, 151.0, 150.2, 137.6, 135.6, 129.2, 128.0, 125.8, 125.5, 125.0, 122.7, 112.1, 39.0, 30.0, 17.77, 17.60, 14.8, 11.43, 11.28. HRMS (ESI) (+ve ion) m/z calcd for $[C_{25}H_{34}N_7S_2]^+$: 496.2317 $[M + H]^+$; found, 496.2310. Elemental analysis calcd (%) for $C_{25}H_{33}N_7S_2{\cdot}H_2O{\cdot}$MeCN: C 58.46, H, 6.53, N, 20.20; found C 58.17, H 6.53, N 20.26.

Synthesis of H_2L^6. To a flask charged with DTSE-*N*-methyl-*N*-phenyl (83 mg, 0.22 mmol) and (*E*)-4-amino-4′-dimethylaminostilbene (55 mg, 0.23 mmol) was added acetonitrile (5 mL), and the

https://dx.doi.org/10.1021/acs.inorgchem.0c01520
Inorg. Chem. XXXX, XXX, XXX−XXX

mixture was heated at reflux for 6 h. A yellow precipitate was isolated by hot filtration, washed with acetonitrile and then pentane, and dried at the pump (38 mg, 0.07 mmol, 32%). ^{1}H NMR (400 MHz; DMSO-d_6): δ 10.76 (s, 1H, N*H*), 10.39 (s, 1H, N*H*), 9.89 (s, 1H, N*H*), 8.33 (m, 1H, N*H*), 7.59 (m, 2H, Ar*H*), 7.52 (m, 2H, Ar*H*), 7.43 (m, 2H, Ar*H*), 7.11 (d, $^3J_{HH}$ = 16.3 Hz, 1H, C*H*═CH), 6.97 (d, $^3J_{HH}$ = 16.4 Hz, 1H, CH═C*H*), 6.72 (m, 2H, Ar*H*), 3.60 (m, 2H, CH_2) 2.97 (m, 10H, CH_2, CH_2, N(CH_3)$_2$), 1.15 (t, $^3J_{HH}$ = 7.1 Hz, 3H, CH_3), 0.95 (m, 6H, CH$_3$,CH_3). ^{13}C NMR (101 MHz; DMSO-d_6): δ 177.5, 176.3, 152.0, 150.6, 149.9, 137.3, 135.0, 128.4, 127.5, 125.5, 125.02, 124.98, 123.0, 112.2, 40.0, 38.6, 17.34, 17.16, 14.3, 10.99, 10.85. HRMS (ESI) (+ve ion) m/z calcd for $[C_{26}H_{36}N_7S_2]^+$: 510.2474 $[M + H]^+$; found, 510.2473. Elemental analysis calcd (%) for $C_{26}H_{35}N_7S_2{\cdot}0.2H_2O$: C 60.83, H, 6.95, N, 19.10; found C 60.57, H 6.56, N 19.45.

General Procedure for the synthesis of Cu(II) Complexes H_2L^{1-6}. To a flask charged with ligands H_2L^{1-6} (1 equiv) and $Cu(OAc)_2{\cdot}H_2O$ (1.1 equiv) was added dimethylformamide (2 mL). The reaction mixture was stirred under an atmosphere of N_2. After 2 h H_2O was added to the red mixture and a very fine precipitate was observed which was collected by centrifugation and analyzed by HRMS and elemental analyses.

Synthesis of [CuL^1]. Following the general procedure, the following parameters were obtained: H_2L^1 (100 mg, 0.22 mmol) and $Cu(OAc)_2.H_2O$ (46 mg, 0.25 mmol); the product was isolated as a brown powder (93 mg, 0.18 mmol, 82%). HRMS (ESI) (+ve ion) m/z calcd for $[C_{22}H_{26}CuN_7S_2]^+$: 515.0987 $[M + H]^+$; found, 515.0974. Elemental analysis calcd (%) for $C_{22}H_{25}CuN_7S_2{\cdot}0.5H_2O$: C 50.41, H 5.00, N 18.71; found C 50.19, H 5.14, N 18.60.

Synthesis of [CuL^2]. Following the general procedure, the following parameters were obtained: H_2L^2 (97 mg, 0.21 mmol) and $Cu(OAc)_2{\cdot}H_2O$ (48 mg, 0.26 mmol); the product was isolated as a brown powder (101 mg, 0.19 mmol, 91%). HRMS (ESI) (+ve ion) m/z calcd for $[C_{23}H_{28}CuN_7S_2]^+$: 529.1144 $[M + H]^+$; found, 529.1130. Elemental analysis calcd (%) for for $C_{23}H_{27}CuN_7S_2$: C 52.20, H 5.14, N 18.53; found C 52.01, H, 5.20, N 18.60.

Synthesis of [CuL^3]. Following the general procedure, the following parameters were obtained: H_2L^3 (47 mg, 0.096 mmol) and $Cu(OAc)_2.H_2O$ (22 mg, 0.11 mmol); the product was isolated as a brown powder (39 mg, 0.073 mmol, 76%). HRMS (ESI) (+ve ion) m/z calcd for $[C_{24}H_{30}CuN_7S_2]^+$: 543.1300 $[M + H]^+$; found, 543.1291. Elemental analysis calcd (%) for $C_{24}H_{29}CuN_7S_2{\cdot}H_2O$: C 51.36, H 5.57, N 17.47; found C 51.34; H 5.20; N 17.86.

Synthesis of [CuL^4]. Following the general procedure, the following parameters were obtained: H_2L^4 (23 mg, 0.046 mmol) and $Cu(OAc)_2{\cdot}H_2O$ (10 mg, 0.052 mmol); the product was isolated as a brown powder (24 mg, 0.043 mmol, 93%). HRMS (ESI) (+ve ion) m/z calcd for $[C_{25}H_{32}CuN_7S_2]^+$: 557.1457 $[M + H]^+$; found, 557.1444. Elemental analysis calcd (%) for $C_{25}H_{31}CuN_7S_2$: C 53.89, H 5.61, N 17.60; found C 53.54, H 5.90, N 17.62.

Synthesis of [CuL^5]. Following the general procedure, the following parameters were obtained: H_2L^5 (14 mg, 0.027 mmol) and $Cu(OAc)_2.H_2O$ (7.3 mg, 0.037 mmol); the product was isolated as a brown powder (12 mg, 0.022 mmol, 81%). HRMS (ESI) (+ve ion) m/z calcd for $[C_{25}H_{32}CuN_7S_2]^+$: 557.1457 $[M + H]^+$; found, 557.1444. Elemental analysis calcd (%) for $C_{25}H_{31}CuN_7S_2{\cdot}0.5H_2O$: C 52.24, H 6.03, N 17.25; found, C 53.24, H 5.65, N 17.13.

Synthesis of [CuL^6]. Following the general procedure, the following parameters were obtained: H_2L^6 (5 mg, 0.009 mmol) and $Cu(OAc)_2.H_2O$ (2 mg, 0.095 mmol); the product was isolated as a brown powder (4.5 mg, 0.010 mmol, 78%). HRMS (ESI) (+ve ion) m/z calcd for $[C_{26}H_{34}CuN_7S_2]^+$: 571.1613 $[M + H]^+$; found, 571.1600. Elemental analysis calcd (%) for $C_{26}H_{33}CuN_7S_2$: C 54.67, H 5.82, N 17.16; found, C 54.43, H 5.94, N 17.01.

Synthesis of [^{64}Cu]CuL$^{1-6}$. [^{64}Cu]$CuCl_2$ in 0.1 M HCl was obtained from was obtained from the Sir Charles Gardiner Hospital Radiopharmaceutical Production and Development Centre (Perth, WA, Australia). Aliquots of the [^{64}Cu]$CuCl_2$ solution (10 μL, 12.5 MBq) were buffered with sodium acetate (1 M, 10 μL, pH 4.5); each of the ligands H_2L^{1-6} (2 μg in 10 μL of DMSO) was added, and the reaction mixture was left to stand at room temperature for 30 min. Then, an aliquot was analyzed by radio-HPLC to determine the radiochecmical yield and purity (0−100% of buffer B to A at 1 mL/min over 15 min, A = 0.05% TFA in Milli-Q and B = in 0.05% TFA in acetonitrile, Luna C18 column 4.6 × 150 mm, 5 μm). The log($D_{7.4}$) for each tracer was measured according to reported procedure. For log $D_{7.4}$ measurements, an aliquot (2 μL) of the radioactive reaction mixture was added to a partition of 1-octanol (500 μL) that had been saturated with PBS and to PBS (498 μL) that had been saturated with 1-octanol. The mixture was vortexed briefly and then allowed to separate over the course of 30 min to 1 h. An aliquot (400 μL) of the 1-octanol layer was taken and repartitioned against PBS (400 μL). The mixture was then vortexed briefly and allowed to separate over 30 min, and an aliquot (2 μL) of each layer was collected; the amount of radioactivity in each layer was quantified using a Capintec (Captus 4000e) gamma counter. Log $D_{7.4}$ was then calculated by calculating the $\log_{10}$ of the ratio of the counts between the 1-octanol layer and the PBS layer. Each partition was repeated in triplicate and reported as the average.

***In Vivo* Biodistribution of [^{64}Cu]CuL^2 and [^{64}Cu]CuL^6 in Balb/c Mice.** All animal experiments were performed with the approval of the Peter MacCallum Cancer Centre Animal Experimentation Ethics Committee and in accordance with the Australian code for the care and use of animals for scientific purposes, eighth edition, 2013. For *in vivo* biodistribution studies [^{64}Cu][Cu**L**^{2}] and [^{64}Cu][Cu**L**^{6}] were radiolabeled using the above procedure, and the final doses were diluted in 0.1 M ammoniumn acetate buffer containing 10% DMSO and 8% ethanol (pH 7.0, 3−4 MBq, 150 μL each). Mice (Balb/c) (n = 3 for each time point) were injected via an intravenous tail vein injection. Mice were euthanized at each time point. Organs of interest were removed and weighed, and the radioactivity present in each organ was quantified using a Capintec (Captus 4000e) gamma counter. The results are presented as the percentage injected activity per gram of tissue (% IA/g).

UV−vis Spectroscopy and Glutathione (GSH) Challenge. UV−vis and fluorescence spectra were recorded in DMSO using (5 μM) solutions of the complexes [Cu**L**$^{1-6}$]. A broad absorption centered at λ_{max} = 480 nm due to characteristic MLCT transitions that occur in typical bis(thiosemicarbazonato)copper(II) complexes was observed (Figure S19). The emission spectra (λ_{ex} = 365 nm) shows strong emission bands centered at 420−440 nm for all samples attributed to typical fluorescence from the stilbene functional group (Figure S20). The stability of the complexes was tested in the presence of glutathione as the reductant. Stock solutions (1 mM) of complexes [Cu**L**$^{1-6}$] were prepared in DMSO and then diluted in PBS to a final concentration of 10 μM in PBS with 20% DMSO. Aliquots of the samples were treated with GSH (1 mM) for 1 h at RT, and UV−vis spectra were recorded for both treated and untreated samples where no change was observed (Figure S21).

***In Vitro* Aβ Binding Assays.** Synthetic Aβ_{1-40} (500 μg, Bachem, 4014442) was dissolved in HFIP (500 μL), and the mixture was incubated on ice for 1 h and then left in a fumehood to evaporate overnight followed by drying by high speed vacuum centrifugation to remove residual HFIP and moisture. The peptide was dissolved in 60 mM NaOH (100 μL) and incubated for 5 min at room temperature. Then, Milli-Q water (350 μL) was added, the mixture was ultrasonicated for 5 min on ice. The solution was buffered with 10 × PBS (pH 7.4, 50 μL) and centrifuged for 5 min, and an aliquot of supernatant was analyzed by UV spectrometry to determine the concentration (λ_{abs} = 214, ε = 94526 M^{-1} cm^{-1}); the concentration was found to be 148 μM. Stock solutions of ThT (1 mM in PBS) and complexes [Cu**L**$^{1-6}$] (1 mM in DMSO) were prepared freshly; final samples (100 μL, in triplicates) were prepared on ice by mixing Aβ_{1-40} (final concentration, 4 μM), ThT (final concentration, 4 μM), and [Cu**L**$^{1-6}$] (final concentration, 1 μM), and the control consisted of Aβ_{1-40} (final concentration, 4 μM) and ThT (final concentration, 4 μM). The samples were prepared on a 96-well plate and incubated at 37 °C in a FLUOstar Omega filter-based multimode microplate reader. The ThT fluorescence intensity (440/480 nm excitation/emission filters) of each sample was recorded every 10 min with orbital shaking before each cycle.

https://dx.doi.org/10.1021/acs.inorgchem.0c01520
Inorg. Chem. XXXX, XXX, XXX−XXX

For the assay with preformed fibrils, a stock solution of $A\beta_{1-40}$ (100 μM) was gently agitated for 48 h in PBS at 37 °C to promote the formation of Aβ fibrils. Then, the solution was treated with an equivalent amount of ThT (100 μM) for 1 h. The solution was diluted, and an aliquot (5 μM fibrils) was treated with the copper complexes, [CuL^2] and [CuL^6] as well as the free ligands H_2L^2 and H_2L^6 (1 μM and 0.1 μM) for 1 h at 37 °C. Then, the ThT fluorescence intensity of each sample was recorded using the plate reader.

TEM Imaging of Aβ Fibrils. A stock solution of $A\beta_{1-40}$ (100 μM) was incubated in PBS at 37 °C and agitated at 300 rpm for 48 h to promote the formation of fibrils, which was confirmed using ThT fluorescence response. The fibrils (10 μM) were then incubated and agitated with the Cu(II) complexes (10 nM) for 2 h at 37 °C. The solutions were spotted onto 300-mesh carbon-coated copper grids and allowed to incubate for 2 min; excess solution was blotted off. Samples were then negatively stained with uranyl acetate (0.5% w/v, 2 min) and analyzed on a FEI Tecnai F20 TEM transmission electron microscope at a voltage of 200 kV.

Treatment of Human AD Brain Tissues with [CuL^2] and [CuL^6]. Experiments using post-mortem human brain tissue were performed with the approval of the University of Melbourne, Faculty of Science Human Ethics Advisory Group (Ethics ID 1341145). Human brain tissues (provided by the Victorian Brain Bank, Melbourne, Australia) were collected by autopsy from the frontal cortex and preserved by formalin fixation and paraffin embedding. The brain tissue sections (7 μm) were first deparaffined (xylene, 3 × 2 min) and then rehydrated (soaked for 2 min in a series of 100%, 90%, 70%, and 0% v/v ethanol/water). The hydrated tissue sections were washed in phosphate buffer saline (PBS, 5 min). Autofluorescence of the tissue was quenched using potassium permanganate ($KMnO_4$) (0.25% in PBS, 20 min), and the sections were washed with potassium metabisulfite and oxalic acid (1% in PBS) until the brown color was removed, followed by washing with PBS (3 × 2 min). The sections were blocked with bovine serum albumin (2% BSA in PBS, pH 7.0, 10 min) and covered with a solution of [CuL^2] or [CuL^6] complexes (10 μM in 15% v/v DMSO/PBS, 10 min). The sections were treated with BSA again (4 min) to remove any Cu(II) complex nonspecifically bound to the tissue and then were washed with PBS (3 × 2 min) and deionized water. The coverslips were mounted using Dako fluorescence mounting medium (Agilent/Dako, cat# S3023). Fluorescence images were visualized using a Leica DM IL LED microscope.

X-ray Crystallography. The molecular structure of [CuL^1] was confirmed by X-ray crystallography. Single crystals suitable for X-ray diffraction were obtained by slow evaporation of compound dissolved in DMF. Intensity data for CuL^1 were collected with an Oxford Diffraction SuperNova CCD diffractometer using Cu−Kα radiation, and the temperature during all data collections was maintained at 130.0(1) K using an Oxford Cryosystems cooling device. The structure was solved by direct methods using SHELXT and refined using the least-squares method using SHELXL.[65,66] Thermal ellipsoid plots were generated using the program Mercury integrated with the WINGX suite of programs.[67] Crystal data for CuL^1: $C_{22}H_{25}CuN_7S_2Cu\cdot$(DMF) M = 588.24, T = 130.0(2) K, λ = 1.54184 Å, monoclinic, space group $P2_1/c$, a = 9.1130(2) Å, b = 8.9380(2) Å, c = 33.5671(7)) Å, β = 96.493(2)°, V = 2716.57(10) Å^3, Z = 4, D_c = 1.438 Mg M^{-3} μ(Cu−K α) = 2.852 mm^{-1}, F(000) = 504, crystal size = 0.27 × 0.14 × 0.03 mm; θ_{max} = 76.54°, 11453 reflections measured, 5314 independent reflections (R_{int} = 0.0262), the final R = 0.0358 [$I > 2\sigma(I)$, 4432 data] and $wR(F^2)$ = 0.1032 (all data), GOOF = 1.055; CCDC accession code 1982494.

■ ASSOCIATED CONTENT

Supporting Information

The Supporting Information is available free of charge at https://pubs.acs.org/doi/10.1021/acs.inorgchem.0c01520.

^{1}H NMR spectra; HR-ESMS spectra; absorption/emmision spectroscopy and GSH challenge; electrochemistry of free ligands; and biodistribution analyses (PDF)

Accession Codes

CCDC 1982494 contains the supplementary crystallographic data for this paper. These data can be obtained free of charge via www.ccdc.cam.ac.uk/data_request/cif, or by emailing data_request@ccdc.cam.ac.uk, or by contacting The Cambridge Crystallographic Data Centre, 12 Union Road, Cambridge CB2 1EZ, UK; fax: +44 1223 336033.

■ AUTHOR INFORMATION

Corresponding Author

Paul S. Donnelly − *School of Chemistry and Bio21 Molecular Science and Biotechnology Institute, University of Melbourne, Parkville, Victoria 3010, Australia;* orcid.org/0000-0001-5373-0080; Email: pauld@unimelb.edu.au

Authors

Asif Noor − *School of Chemistry and Bio21 Molecular Science and Biotechnology Institute, University of Melbourne, Parkville, Victoria 3010, Australia*

David J. Hayne − *School of Chemistry and Bio21 Molecular Science and Biotechnology Institute, University of Melbourne, Parkville, Victoria 3010, Australia;* orcid.org/0000-0003-2756-9427

SinChun Lim − *School of Chemistry and Bio21 Molecular Science and Biotechnology Institute, University of Melbourne, Parkville, Victoria 3010, Australia*

Jessica K. Van Zuylekom − *Research Division, Peter MacCallum Cancer Centre, Melbourne, Victoria 3000, Australia*

Carleen Cullinane − *Research Division, Peter MacCallum Cancer Centre, Melbourne, Victoria 3000, Australia; The Sir Peter MacCallum Department of Oncology, University of Melbourne, Parkville, Victoria 3010, Australia*

Peter D. Roselt − *Centre for Cancer Imaging, Peter MacCallum Cancer Centre, Melbourne, Victoria 3000, Australia*

Catriona A. McLean − *The Florey Institute of Neuroscience and Mental Health, University of Melbourne, Parkville, Victoria 3010, Australia; Department of Anatomical Pathology, The Alfred Hospital, Victoria 3181, Australia*

Jonathan M. White − *School of Chemistry and Bio21 Molecular Science and Biotechnology Institute, University of Melbourne, Parkville, Victoria 3010, Australia;* orcid.org/0000-0002-0707-6257

Complete contact information is available at: https://pubs.acs.org/10.1021/acs.inorgchem.0c01520

Funding

The Australian Research Council is acknowledged for financial support (DP160100288, LP150100656).

Notes

The authors declare no competing financial interest.

■ ACKNOWLEDGMENTS

The human brain tissue was provided by The Victorian Brain Bank Network. We acknowledge the Mass Spectrometry and Proteomics Facility (MSPF) at the Bio21 Institute, University of Melbourne, for the use of their mass spectrometer and HPLC systems. Professor Rodney J. Hicks (Peter MacCallum Cancer Centre) is thanked for his generous support of this research by provision of radiochemistry facilities. We thank

https://dx.doi.org/10.1021/acs.inorgchem.0c01520
Inorg. Chem. XXXX, XXX, XXX−XXX

Susan Jackson (Peter MacCallum Cancer Centre) for her technical expertise in performing the *in vivo* biodistribution study.

REFERENCES

(1) Glenner, G. G.; Wong, C. W. Alzheimer's disease and Down's syndrome: sharing of a unique cerebrovascular amyloid fibril protein. *Biochem. Biophys. Res. Commun.* **1984**, *122*, 1131−5.
(2) Glenner, G. G.; Wong, C. W. Alzheimer's disease: initial report of the purification and characterization of a novel cerebrovascular amyloid protein. *Biochem. Biophys. Res. Commun.* **1984**, *120*, 885−90.
(3) Glenner, G. G.; Wong, C. W.; Quaranta, V.; Eanes, E. D. The amyloid deposits in Alzheimer's disease: their nature and pathogenesis. *Appl. Pathol* **1984**, *2*, 357−369.
(4) Masters, C. L.; Simms, G.; Weinman, N. A.; Multhaup, G.; McDonald, B. L.; Beyreuther, K. Amyloid plaque core protein in Alzheimer disease and Down syndrome. *Proc. Natl. Acad. Sci. U. S. A.* **1985**, *82*, 4245−4249.
(5) Hardy, J.; Selkoe, D. J. The amyloid hypothesis of Alzheimer's disease: progress and problems on the road to therapeutics. *Science* **2002**, *297*, 353−356.
(6) Selkoe, D. J. Resolving controversies on the path to Alzheimer's therapeutics. *Nat. Med.* **2011**, *17*, 1060−1065.
(7) Mathis, C. A.; Bacskai, B. J.; Kajdasz, S. T.; McLellan, M. E.; Frosch, M. P.; Hyman, B. T.; Holt, D. P.; Wang, Y.; Huang, G.-F.; Debnath, M. L.; Klunk, W. E. A lipophilic thioflavin-T derivative for positron emission tomography (PET) imaging of amyloid in brain. *Bioorg. Med. Chem. Lett.* **2002**, *12*, 295−298.
(8) Mathis, C. A.; Mason, N. S.; Lopresti, B. J.; Klunk, W. E. Development of positron emission tomography *β*-amyloid plaque imaging agents. *Semin. Nucl. Med.* **2012**, *42*, 423−32.
(9) Villemagne, V. L.; Dore, V.; Burnham, S. C.; Masters, C. L.; Rowe, C. C. Imaging tau and amyloid-*β* proteinopathies in Alzheimer disease and other conditions. *Nat. Rev. Neurol.* **2018**, *14*, 225−236.
(10) Fantoni, E.; Collij, L.; Alves, I. L.; Buckley, C.; Farrar, G. The Spatial-Temporal Ordering of Amyloid Pathology and Opportunities for PET Imaging. *J. Nucl. Med.* **2020**, *61*, 166−171.
(11) Zhang, W.; Oya, S.; Kung, M.-P.; Hou, C.; Maier, D. L.; Kung, H. F. F-18 Polyethyleneglycol stilbenes as PET imaging agents targeting A*β* aggregates in the brain. *Nucl. Med. Biol.* **2005**, *32*, 799−809.
(12) Kung, H. F.; Choi, S. R.; Qu, W.; Zhang, W.; Skovronsky, D. 18F Stilbenes and Styrylpyridines for PET Imaging of Abeta Plaques in Alzheimer's Disease: A Miniperspective. *J. Med. Chem.* **2010**, *53*, 933−941.
(13) Sabri, O.; Seibyl, J.; Rowe, C.; Barthel, H. Beta-amyloid imaging with florbetaben. *Clinical and Translational Imaging* **2015**, *3*, 13−26.
(14) Ikawa, M.; Okazawa, H.; Tsujikawa, T.; Matsunaga, A.; Yamamura, O.; Mori, T.; Hamano, T.; Kiyono, Y.; Nakamoto, Y.; Yoneda, M. Increased oxidative stress is related to disease severity in the ALS motor cortex: A PET study. *Neurology* **2015**, *84*, 2033−2039.
(15) Neishi, H.; Ikawa, M.; Okazawa, H.; Tsujikawa, T.; Arishima, H.; Kikuta, K.; Yoneda, M. Precise Evaluation of Striatal Oxidative Stress Corrected for Severity of Dopaminergic Neuronal Degeneration in Patients with Parkinson's Disease: A Study with ^{62}Cu-ATSM PET and ^{123}I-FP-CIT SPECT. *Eur. Neurol.* **2017**, *78*, 161−168.
(16) Toriihara, A.; Ohtake, M.; Tateishi, K.; Hino-Shishikura, A.; Yoneyama, T.; Kitazume, Y.; Inoue, T.; Kawahara, N.; Tateishi, U. Prognostic implications of ^{62}Cu-diacetyl-bis (N4-methylthiosemicarbazone) PET/CT in patients with glioma. *Ann. Nucl. Med.* **2018**, *32*, 264−271.
(17) Tsuchiya, J.; Yoneyama, T.; Ohtake, M.; Tateishi, K.; Bae, H.; Kishino, M.; Tateishi, U. Redox reaction and clinical outcome of primary diffuse large B-cell lymphoma of the central nervous system: Prognostic role of metabolic and textural parameters of ^{62}Cu-diacetyl-bis (N4-methylthiosemicarbazone) PET/computed tomography in a small patient cohort. *Nucl. Med. Commun.* **2020**, *41*, 567−574.
(18) McCarthy, D. W.; Bass, L. A.; Cutler, P. D.; Shefer, R. E.; Klinkowstein, R. E.; Herrero, P.; Lewis, J. S.; Cutler, C. S.; Anderson, C. J.; Welch, M. J. High purity production and potential applications of copper-60 and copper-61. *Nucl. Med. Biol.* **1999**, *26*, 351−358.
(19) Hickey, J. L.; Lim, S. C.; Hayne, D. J.; Paterson, B. M.; White, J. M.; Villemagne, V. L.; Roselt, P.; Binns, D.; Cullinane, C.; Jeffery, C. M.; Price, R. I.; Barnham, K. J.; Donnelly, P. S. Diagnostic Imaging Agents for Alzheimer's Disease: Copper Radiopharmaceuticals that Target A*β* Plaques. *J. Am. Chem. Soc.* **2013**, *135*, 16120−16132.
(20) McInnes, L. E.; Noor, A.; Kysenius, K.; Cullinane, C.; Roselt, P.; McLean, C. A.; Chiu, F. C. K.; Powell, A. K.; Crouch, P. J.; White, J. M.; Donnelly, P. S. Potential Diagnostic Imaging of Alzheimer's Disease with Copper-64 Complexes That Bind to Amyloid-*β* Plaques. *Inorg. Chem.* **2019**, *58*, 3382−3395.
(21) Fujibayashi, Y.; Taniuchi, H.; Yonekura, Y.; Ohtani, H.; Konishi, J.; Yokoyama, A. Copper-62-ATSM: a new hypoxia imaging agent with high membrane permeability and low redox potential. *J. Nucl. Med.* **1997**, *38*, 1155−1160.
(22) Vavere, A. L.; Lewis, J. S. A radiopharmaceutical for the PET imaging of hypoxia. *Dalton Trans.* **2007**, 4893−4902.
(23) Lim, S.; Paterson, B. M.; Fodero-Tavoletti, M. T.; O'Keefe, G. J.; Cappai, R.; Barnham, K. J.; Villemagne, V. L.; Donnelly, P. S. A copper radiopharmaceutical for diagnostic imaging of Alzheimer's disease: a bis(thiosemicarbazonato)copper(II) complex that binds to amyloid-*β* plaques. *Chem. Commun.* **2010**, *46*, 5437−5439.
(24) Winkelmann, D. A.; Bermke, Y.; Petering, D. H. Comparative properties of the antineoplastic agent, 3-ethoxy-2-oxobutyraldehyde bis(thiosemicarbazonato) copper(II) and related chelates. Linear free energy correlations. *Bioinorg. Chem.* **1974**, *3*, 261−77.
(25) Wada, K.; Fujibayashi, Y.; Tajima, N.; Yokoyama, A. Cu-ATSM, an intracellular-accessible superoxide dismutase (SOD)-like copper complex: evaluation in an ischemia-reperfusion injury model. *Biol. Pharm. Bull.* **1994**, *17*, 701−704.
(26) Dearling, J. L. J.; Blower, P. J. Redox-active metal complexes for imaging hypoxic tisssues: structure-activity relationships in Cu(II) bis(thiosemicarbazone) complexes. *Chem. Commun.* **1998**, 2531.
(27) Dearling, J. L. J.; Lewis, J. S.; Mullen, G. D.; Welch, M. J.; Blower, P. J. Copper bis(thiosemicarbazone) complexes as hypoxia imaging agents: structure-activity relationships. *JBIC, J. Biol. Inorg. Chem.* **2002**, *7*, 249−259.
(28) Cowley, A. R.; Dilworth, J. R.; Donnelly, P. S.; Labisbal, E.; Sousa, A. An Unusual Dimeric Structure of a Cu(I) Bis-(thiosemicarbazone) Complex: Implications for the Mechanism of Hypoxic Selectivity of the Cu(II) Derivatives. *J. Am. Chem. Soc.* **2002**, *124*, 5270−5271.
(29) Xiao, Z.; Donnelly, P. S.; Zimmermann, M.; Wedd, A. G. Transfer of Copper between Bis(thiosemicarbazone) Ligands and Intracellular Copper-Binding Proteins. Insights into Mechanisms of Copper Uptake and Hypoxia Selectivity. *Inorg. Chem.* **2008**, *47*, 4338−4347.
(30) Donnelly, P. S.; Caragounis, A.; Du, T.; Laughton, K. M.; Volitakis, I.; Cherny, R. A.; Sharples, R. A.; Hill, A. F.; Li, Q.-X.; Masters, C. L.; Barnham, K. J.; White, A. R. Selective Intracellular Release of Copper and Zinc Ions from Bis(thiosemicarbazonato) Complexes Reduces Levels of Alzheimer Disease Amyloid-*β* Peptide. *J. Biol. Chem.* **2008**, *283*, 4568−4577.
(31) Price, K. A.; Crouch, P. J.; Volitakis, I.; Paterson, B. M.; Lim, S.; Donnelly, P. S.; White, A. R. Mechanisms Controlling the Cellular Accumulation of Copper Bis(thiosemicarbazonato) Complexes. *Inorg. Chem.* **2011**, *50*, 9594−9605.
(32) Mathias, C. J.; Bergmann, S. R.; Green, M. A. Species-Dependent Binding of Copper(II) Bis(Thiosemicarbazone) Radiopharmaceuticals to Serum Albumin. *J. Nucl. Med.* **1995**, *36* (8), 1451−1455.
(33) Green, M. A.; Mathias, C. J.; Willis, L. R.; Handa, R. K.; Lacy, J. L.; Miller, M. A.; Hutchins, G. D. Assessment of Cu-ETS as a PET radiopharmaceutical for evaluation of regional renal perfusion. *Nucl. Med. Biol.* **2007**, *34*, 247−255.

https://dx.doi.org/10.1021/acs.inorgchem.0c01520
Inorg. Chem. XXXX, XXX, XXX−XXX

(34) Basken, N. E.; Green, M. A. Cu(II) bis(thiosemicarbazone) radiopharmaceutical binding to serum albumin: further definition of species dependence and associated substituent effects. *Nucl. Med. Biol.* **2009**, *36*, 495−504.
(35) Basken, N. E.; Mathias, C. J.; Green, M. A. Elucidation of the human serum albumin (HSA) binding site for the Cu-PTSM and Cu-ATSM radiopharmaceuticals. *J. Pharm. Sci.* **2009**, *98*, 2170−2179.
(36) Paterson, B. M.; Karas, J. A.; Scanlon, D. B.; White, J. M.; Donnelly, P. S. Versatile New Bis(thiosemicarbazone) Bifunctional Chelators: Synthesis, Conjugation to Bombesin(7−14)-NH_2, and Copper-64 Radiolabeling. *Inorg. Chem.* **2010**, *49*, 1884−1893.
(37) Buncic, G.; Donnelly, P. S.; Paterson, B. M.; White, J. M.; Zimmermann, M.; Xiao, Z.; Wedd, A. G. A Water-soluble bis-(thiosemicarbazone) ligand. A sensitive probe and metal buffer for zinc. *Inorg. Chem.* **2010**, *49*, 3071−3073.
(38) Buncic, G.; Hickey, J. L.; Schieber, C.; White, J. M.; Crouch, P. J.; White, A. R.; Xiao, Z.; Wedd, A. G.; Donnelly, P. S. Water-soluble Bis(thiosemicarbazonato)copper(II) Complexes. *Aust. J. Chem.* **2011**, *64*, 244−252.
(39) Hickey, J. L.; James, J. L.; Henderson, C. A.; Price, K. A.; Mot, A. I.; Buncic, G.; Crouch, P. J.; White, J. M.; White, A. R.; Smith, T. A.; Donnelly, P. S. Intracellular Distribution of Fluorescent Copper and Zinc Bis(thiosemicarbazonato) Complexes Measured with Fluorescence Lifetime Spectroscopy. *Inorg. Chem.* **2015**, *54*, 9556−9567.
(40) Blower, P. J.; Castle, T. C.; Cowley, A. R.; Dilworth, J. R.; Donnelly, P. S.; Labisbal, E.; Sowrey, F. E.; Teat, S. J.; Went, M. J. Structural trends in copper(II) bis(thiosemicarbazone) radiopharmaceuticals. *Dalton Trans.* **2003**, 4416−4425.
(41) Holland, J. P.; Aigbirhio, F. I.; Betts, H. M.; Bonnitcha, P. D.; Burke, P.; Christlieb, M.; Churchill, G. C.; Cowley, A. R.; Dilworth, J. R.; Donnelly, P. S.; Green, J. C.; Peach, J. M.; Vasudevan, S. R.; Warren, J. E. Functionalized Bis(thiosemicarbazonato) Complexes of Zinc and Copper: Synthetic Platforms Toward Site-Specific Radiopharmaceuticals. *Inorg. Chem.* **2007**, *46*, 465−485.
(42) Holland, J. P.; Green, J. C.; Dilworth, J. R. Probing the mechanism of hypoxia selectivity of copper bis(thiosemicarbazonato) complexes: DFT calculation of redox potentials and absolute acidities in solution. *Dalton Trans.* **2006**, 783−794.
(43) Waterhouse, R. N. Determination of lipophilicity and its use as a predictor of blood-brain barrier penetration of molecular imaging agents. *Mol. Imaging Biol.* **2003**, *5*, 376−389.
(44) Kannan, P.; Pike, V. W.; Halldin, C.; Langer, O.; Gottesman, M. M.; Innis, R. B.; Hall, M. D. Factors That Limit Positron Emission Tomography Imaging of P-Glycoprotein Density at the Blood-Brain Barrier. *Mol. Pharmaceutics* **2013**, *10*, 2222−2229.
(45) Pike, V. W. Considerations in the Development of Reversibly Binding PET Radioligands for Brain Imaging. *Curr. Med. Chem.* **2016**, *23*, 1818−1869.
(46) Paterson, B. M.; Cullinane, C.; Crouch, P. J.; White, A. R.; Barnham, K. J.; Roselt, P. D.; Noonan, W.; Binns, D.; Hicks, R. J.; Donnelly, P. S. Modification of Biodistribution and Brain Uptake of Copper Bis(thiosemicarbazonato) Complexes by the Incorporation of Amine and Polyamine Functional Groups. *Inorg. Chem.* **2019**, *58*, 4540−4552.
(47) Ikawa, M.; Okazawa, H.; Arakawa, K.; Kudo, T.; Kimura, H.; Fujibayashi, Y.; Kuriyama, M.; Yoneda, M. PET imaging of redox and energy states in stroke-like episodes of MELAS. *Mitochondrion* **2009**, *9*, 144−148.
(48) Ikawa, M.; Okazawa, H.; Kudo, T.; Kuriyama, M.; Fujibayashi, Y.; Yoneda, M. Evaluation of striatal oxidative stress in patients with Parkinson's disease using [^{62}Cu]ATSM PET. *Nucl. Med. Biol.* **2011**, *38*, 945−951.
(49) Di, L.; Rong, H.; Feng, B. Demystifying Brain Penetration in Central Nervous System Drug Discovery. *J. Med. Chem.* **2013**, *56*, 2−12.
(50) Acevedo, K. M.; Hayne, D. J.; McInnes, L. E.; Noor, A.; Duncan, C.; Moujalled, D.; Volitakis, I.; Rigopoulos, A.; Barnham, K. J.; Villemagne, V. L.; White, A. R.; Donnelly, P. S. Effect of Structural Modifications to Glyoxal-bis(thiosemicarbazonato)copper(II) Complexes on Cellular Copper Uptake, Copper-Mediated ATP7A Trafficking, and P-Glycoprotein Mediated Efflux. *J. Med. Chem.* **2018**, *61*, 711−723.
(51) Basken, N. E.; Mathias, C. J.; Lipka, A. E.; Green, M. A. Species dependence of [64Cu]Cu-Bis(thiosemicarbazone) radiopharmaceutical binding to serum albumins. *Nucl. Med. Biol.* **2008**, *35*, 281−286.
(52) Fodero-Tavoletti, M. T.; Villemagne, V. L.; Paterson, B. M.; White, A. R.; Li, Q.-X.; Camakaris, J.; O'Keefe, G.; Cappai, R.; Barnham, K. J.; Donnelly, P. S. Bis (thiosemicarbazonato) Cu-64 Complexes for Positron Emission Tomography Imaging of Alzheimer's Disease. *J. Alzheimer's Dis.* **2010**, *20*, 49−55.
(53) Caldwell, J.; Gardner, I.; Swales, N. An introduction to drug disposition: the basic principles of absorption, distribution, metabolism, and excretion. *Toxicol. Pathol.* **1995**, *23*, 102−14.
(54) Karlgren, M.; Bergstroem, C. A. S. How physicochemical properties of drugs affect their metabolism and clearance. *RSC Drug Discovery Series* **2015**, *49*, 1−26.
(55) Boer, F. Drug handling by the lungs. *Br. J. Anaesth.* **2003**, *91*, 50−60.
(56) McInnes, L. E.; Rudd, S. E.; Donnelly, P. S. Copper, gallium and zirconium positron emission tomography imaging agents: The importance of metal ion speciation. *Coord. Chem. Rev.* **2017**, *352*, 499−516.
(57) Bandara, N.; Sharma, A. K.; Krieger, S.; Schultz, J. W.; Han, B. H.; Rogers, B. E.; Mirica, L. M. Evaluation of 64Cu-Based Radiopharmaceuticals that Target Aβ Peptide Aggregates as Diagnostic Tools for Alzheimer's Disease. *J. Am. Chem. Soc.* **2017**, *139*, 12550−12558.
(58) Sharma, A. K.; Schultz, J. W.; Prior, J. T.; Rath, N. P.; Mirica, L. M. Coordination Chemistry of Bifunctional Chemical Agents Designed for Applications in ^{64}Cu PET Imaging for Alzheimer's Disease. *Inorg. Chem.* **2017**, *56*, 13801−13814.
(59) Hickey, J. L.; Donnelly, P. S. Diagnostic imaging of Alzheimer's disease with copper and technetium complexes. *Coord. Chem. Rev.* **2012**, *256*, 2367−2380.
(60) Hayne, D. J.; Lim, S. C.; Donnelly, P. S. Metal complexes designed to bind to amyloid-β for the diagnosis and treatment of Alzheimer's disease. *Chem. Soc. Rev.* **2014**, *43*, 6701−6715.
(61) Chen, K.; Cui, M. Recent progress in the development of metal complexes as β-amyloid imaging probes in the brain. *MedChemComm* **2017**, *8*, 1393−1407.
(62) McInnes, L. E.; Noor, A.; Roselt, P. D.; McLean, C. A.; White, J. M.; Donnelly, P. S. A Copper Complex of a Thiosemicarbazone-Pyridylhydrazone Ligand Containing a Vinylpyridine Functional Group as a Potential Imaging Agent for Amyloid-β Plaques. *Aust. J. Chem.* **2019**, *72*, 827−834.
(63) Shakya, B.; Yadav, P. N.; Ueda, J.-y.; Awale, S. Discovery of 2-pyridineformamide thiosemicarbazones as potent antiausterity agents. *Bioorg. Med. Chem. Lett.* **2014**, *24*, 458−461.
(64) Jiao, J.; Zhang, X.-R.; Chang, N.-H.; Wang, J.; Wei, J.-F.; Shi, X.-Y.; Chen, Z.-G. A Facile and Practical Copper Powder-Catalyzed, Organic Solvent- and Ligand-Free Ullmann Amination of Aryl Halides. *J. Org. Chem.* **2011**, *76*, 1180−1183.
(65) Sheldrick, G. M. A short history of SHELX. *Acta Crystallogr., Sect. A: Found. Crystallogr.* **2008**, *64*, 112−122.
(66) Sheldrick, G. M. Crystal structure refinement with SHELXL. *Acta Crystallogr., Sect. C: Struct. Chem.* **2015**, *71*, 3−8.
(67) Farrugia, L. J. WinGX and ORTEP for Windows: an update. *J. Appl. Crystallogr.* **2012**, *45*, 849−854.

https://dx.doi.org/10.1021/acs.inorgchem.0c01520
Inorg. Chem. XXXX, XXX, XXX−XXX